Pressure-Stimulated Rock Current as Loading Diorite to Failure: Particular Variation and Holistic Mechanisms

Wenfei Mao[1], Lixin Wu[1], Youyou Xu[1], Rubing Yao[1], Jingchen Lu[1], Licheng Sun[1], and Yuan Qi[1]

[1]Central South University

November 24, 2022

Abstract

The variations in the electric property of loaded rocks are essential in understanding the rock dynamics and fracturing process. Decades of laboratory experiments have revealed different behaviors of stress-stimulated electric current due to the effects of rock types, loading modes, and detection methods. These different behaviors result in difficulties in revealing the underlying physics of electric current in rock and explaining adequately the wide variety of electric precursors measured before rock failure or geohazards. In this study, cubic- and conical-shaped diorite specimens were specially designed and produced to investigate experimentally the characteristics of pressure-stimulated rock current (PSRC) in the process of loading rock specimen to failure. We measured a particular phenomenon of diorite PSRC variation with pressure, that is, PSRC remained nearly stable until the applied stress reached 83%–98% of the failure strength. A remarkable step-like increment in PSRC was uncovered, and drastic oscillations with maximum amplitudes of several hundreds of nA happened one second prior to abrupt rock failure. A holistic mechanism that includes positive hole activation, field emission of electrons due to crack charge separation, and moving charged dislocation was applied to interpret this particular phenomenon. We found that these mechanisms contribute comprehensively rather than individually to the evolution of PSRC. We expect to provide an improved understanding of the underlying physics of PSRC and the variation in rock electric property.

Pressure-Stimulated Rock Current as Loading Diorite to Failure: Particular Variation and Holistic Mechanisms

Wenfei Mao[1,2], Lixin Wu[1,2*], Youyou Xu[1,2], Rubing Yao[1,2], Jingchen Lu[1,2], Licheng Sun[3], and Yuan Qi[1,2]

[1] School of Geoscience and Info-Physics, Central South University, Changsha, 410083, China.

[2] Laboratory of Geo-Hazards Perception, Cognition and Predication, Central South University, Changsha, 410083, China.

[3] School of Resource and Safety Engineering, Central South University, Changsha, 410083, China.

Corresponding author: Lixin Wu (wulx66@csu.edu.cn)

Key Points:

- Pressure-stimulated rock current (PSRC) increases in a step-like way at high stress level
- PSRC oscillates with maximum amplitudes of several hundreds of nA at the very last instant just before rock failure
- Positive hole activation, crack charge separation, and moving charged dislocation contributes comprehensively to the PSRC variations.

Abstract

The variations in the electric property of loaded rocks are essential in understanding the rock dynamics and fracturing process. Decades of laboratory experiments have revealed different behaviors of stress-stimulated electric current due to the effects of rock types, loading modes, and detection methods. These different behaviors result in difficulties in revealing the underlying physics of electric current in rock and explaining adequately the wide variety of electric precursors measured before rock failure or geohazards. In this study, cubic- and conical-shaped diorite specimens were specially designed and produced to investigate experimentally the characteristics of pressure-stimulated rock current (PSRC) in the process of loading rock specimen to failure. We measured a particular phenomenon of diorite PSRC variation with pressure, that is, PSRC remained nearly stable until the applied stress reached 83%–98% of the failure strength. A remarkable step-like increment in PSRC was uncovered, and drastic oscillations with maximum amplitudes of several hundreds of nA happened one second prior to abrupt rock failure. A holistic mechanism that includes positive hole activation, field emission of electrons due to crack charge separation, and moving charged dislocation was applied to interpret this particular phenomenon. We found that these mechanisms contribute comprehensively rather than individually to the evolution of PSRC. We expect to provide an improved understanding of the underlying physics of PSRC and the variation in rock electric property.

Plain Language Summary

Many kinds of electric precursors of rock fracturing or rock failure have been experimentally revealed in past four decades. Therein, the behaviors of stress stimulated electric current of rock materials are influenced by the loading modes and current detection methods; thus, different mechanisms were proposed accordingly. By uniaxially and partly compressing cubic- and conical-shaped diorite specimens to failure, we revealed the paticular and significant variations of rock current before the rock failure, and found that such behaviors were attributed to a combination of several mechanisms rather than a single one. This study exhibits potential use of dynamic signal detection of pressure stimulated rock current and possible precursor identification of rock fracturing.

1 Introduction

Rock dynamic disasters, such as rock bursts and tectonic earthquakes, result originally from deep rock fracturing or rock failure and occur frequently from a deep part of the ground to the surface. Although electric and magnetic phenomena was observed before some volcano and seismic activities (Uyeda et al., 2002), and many geoscientists and rock engineers have attempted to place various sensors in rock mass to search for early warning of the occurrence of rock failure or geohazards (Liao et al., 2003; Meng et al., 2015), it is difficult or ineffective due to the uncertainty of the detected signals and the complexity of the underground environment. Many laboratorial experiments have been performed to investigate the potential electric precursors of rock failure, and they have revealed several electric signals, including charge particles (Enomoto and Hashimoto, 1990, 1992), surface potential (Hadjicontis and Mavromatou, 1994; Yoshida et al., 1997, 1998; Freund, 2002; Li et al., 2020), and electric currents (Hoenig, 1979; Vallianatos et al, 1999; Stavrakas et al., 2004; Triantis et al., 2006, 2012; Freund et al., 2006; Anastasiadis et al., 2007; Li et al., 2015; Li et al., 2021a, 2021b), preceding or accompanying with rock failure. The generation of electric current in stressed rock (called in brief as rock current) is believed to be associated with the micro-fracturing inside the rock volume, and mechanisms including electrokinetic effects (Mizutani et al., 1976), piezoelectricity (Warwich et al., 1982), field emission of electrons (Enomoto and Hashimoto, 1990, 1992), moving charged dislocation (Slifkin, 1993; Hadjicontis and Mavromatou, 1994; Vallianatos and Tzanis,

1998) and peroxy defects activation (Freund, 2002, 2006) have been proposed. In many experiments, such electric signals are measured when the stress applied to the rock sample exceeds the yield stress (Yoshida et al., 1997; Yoshida et al., 1998; Starrakas et al., 2004; Anastasiadis et al., 2007; Li et al., 2015; Pasiou and Triantis, 2017), but other experiments have shown that electric signals are generated immediately upon the application of any significant mechanical load (Freund et al., 2006; Scoville et al., 2015; Li et al., 2021a, 2021b). Thus, proper interpretation and physical understanding of the differences in electric signals are very necessary.

A review of experimental studies in the past three decades, indicates that two major factors are responsible for the differences mentioned above. First, different rock types have different mechanical properties due to the complex mineral compositions and structures of rocks. Thus, even under the same stress condition, rock specimens present different features of electric signals. For instance, in a tri-axial deformation experiment performed by Yoshida et al. (1998), the electric potential on a dry sandstone surface changed markedly prior to dynamic rupture, but such a change was not observed in dry basalt. The researchers concluded that the piezoelectric effect is the dominant sources of precursory electric signals. Many other experiments have demonstrated that a marble sample emits observable pressure-stimulated rock currents (PSRC) when the progressive uniaxial stress exceeds its linear elasticity limit, and PSRC increases considerably and reaches the maximum value in the vicinity of rock failure (Stavrakas et al., 2004). However, similar experiments on sandstone have demonstrated that weak currents are generated instantaneously when a load is applied initially, and PSRC corresponds well to the stress variations (Li et al., 2021b).

Second, applying different loading and detection modes also influences the detected electric signals in experiments. Figure 1 illustrates three classic loading modes that were commonly applied in the past three decades. In the early 1990s, Enomoto and Hashimoto (1990; 1992) measured the emission of charged particles from rocks undergoing indentation fracturing (Fig. 1a). Given that the indenter served as an electrode, the collected charged particles were highly associated with indentation fracturing; thus, intensive electric signals were concentrated where strong acoustic signals appeared. The amounts of detected electrons and negative ions were higher than that of positive ions when rock cracking occurred around the indenter. Figure 1b shows the most widely used loading mode in rock mechanics experiments, in which the entire rock specimen is loaded. Aside from the effects caused by rock types, many other factors, including loading rate (Hadjicontis and Mavromatou, 1994; Li et al., 2020), moisture of rock specimens (Yoshida et al., 1998; Saltas et al., 2018), Young modulus of rock specimens (Stavrakas et al., 2004; Triantis et al., 2006; Li et al., 2020), strain rate (Triantis et al., 2012), and deformation stage (Li et al., 2021b), have been experimentally confirmed to exert remarkable impacts on PSRC or electric potentials. However, the position of electrodes pasted or mounted on a specimen may also affect experimental results. For instance, when the electrodes are pasted on the side surface of a sandstone specimen (Li et al., 2021b), PSRC initially increases rapidly then decreases slowly a few seconds later; afterward, PSRC increases very slowly until it approaches final failure and reaches the maximum when rupture occurs. Meanwhile, when the electrodes are pasted on the press head of the loading machine (Li et al., 2020), the PSRC variation is divided into three stages, namely, including rapid growth, slow growth, and approaching the peak. As shown in Fig. 1c, the partly loading and detection mode was first adopted by Enomoto and Hashimoto in 1992 by considering the ignorable distance between the initial rock fracturing (usually in deep Earth) and ground surface or the stress gradients from concentration zone to relaxation zone; this mode has been developed and widely used since 2002 (Freund, 2002, 2006, 2009; Scoville et al., 2015; Li et al., 2021a). When only one end or a sub-volume of a rock specimen is subjected to external loads, detectable electric currents or potentials can be measured on the other end or in the stress-free section. Usually, the electric signals are generated immediately upon the application of any significant mechanical load. However, under the influence of the stress concentration effect, macroscopic fracture of a specimen in the third mode (Fig. 1c) occurs initially along the press head edge, and the stress of the rock volume is much less than the rock failure strength. Thus, previous experiments have mainly focused on the elastic deformation phase of rocks, and the evolution of electric signals with sufficient fracturing of rock sub-volume has rarely been investigated and remains unclear.

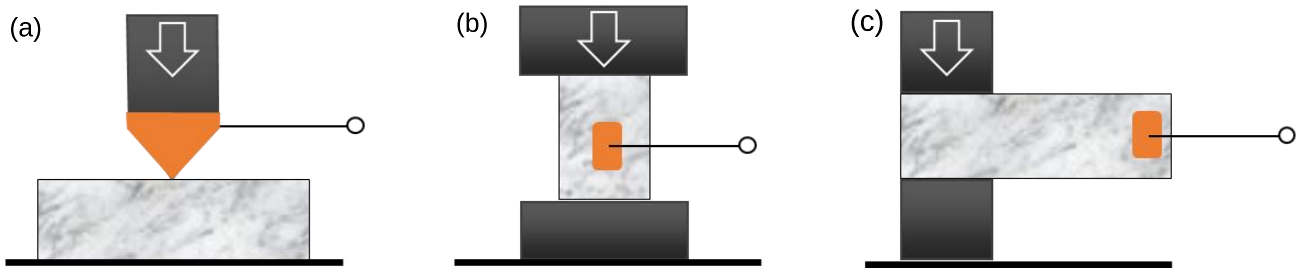

Figure 1. **Schematic of three classic loading modes applied in experiments to detect electric charges generated from rock specimens.** The orange legends represent the commonly applied position of electrodes**. (a)** Indentation loading at one point. **(b)** Loading over the entire cross section. **(c)** Loading partly on one end or a sub-volume.

The variation in electric signals detected from loaded rock specimens is a reflection of the generation and redistribution of charge carries inside rock volumes or on rock surfaces. The inhomogeneous mechanical property of rock specimens and the position of electrodes placed influence the features of detected electric signals. The acoustic emission (AE) detection technique is often used to investigate the relationship between micro-fracturing events and electric signals because the electrification by micro-fracturing is generally considered as the predominate mechanism (Stergiopoulos et al., 2013; Pasiou and Triantis, 2017; Saltas et al., 2018). However, during the loading of a rock specimen, the received AE signals reflect all of the micro-fracturing events occurring inside the entire rock volume, whereas the electrodes pasted on the sample surface generally receive the electric signals induced by nearby opening fractures. The relation between AE and electric signals entails much uncertainty and needs to be investigated further.

This study focused on the third loading mode (Fig. 1c) and aim to clarify the PSRC precursors of rocks partly compressed to fracturing. First, a special-shaped rock specimen was prepared to reduce or eliminate the stress concentration effect, and ensure that the loaded sub-volume could be broken sufficiently. Second, progressive compression was applied until rock failure occurred. During the progressive compression, the PSRC from the entire loaded sub-volume to the unloaded upper part and the AE signals were recorded simultaneously. Lastly, the holistic mechanisms of diorite PSRC were examined.

2 Materials and Methods

2.1 Specimen preparation

Gray diorite, from Fujian Province, China, was used to create the rock specimens. The thin section of the diorite indicates that the diorite is composed of 60% plagioclase, 10% potassium feldspar, 10% pyroxene, and 10% –15% biotite and amphibole (Fig. S1a). In contrast to granite that was commonly adopted in previous experiments, diorite was used in our experiment for three reasons. First, the sizes of the mineral grains in diorite are relatively uniform, and the mechanical property under external loading is homogeneous. Second, few quartz grains are contained in diorite, so the piezoelectric effect on the electric signals can be excluded to reduce the uncertainty in data analysis. Lastly, the proxy defect is common in diorite, which is also a typical igneous rock like granite. Thus, PSRC can be measured due to P-hole activation by compressive stress even if no other mechanism is involved. To reduce or eliminate the stress concentration effect along the press head edge and ensure that the loaded rock sub-volume could be fractured sufficiently, we created a bar-shaped rock specimen with a conical head, as shown in Fig. S1b. The lower part is for uniaxial and compressive loading, and the upper conical part is unloaded and provides a small top plane. For uniaxial compressive loading, the “unparallelism” of two loading surfaces was less than

0.05mm. In addition, the surface of specimen was polished with 400-mesh sandpaper. To prevent water from affecting the rock specimen, we placed them in an oven whose temperature increased to 120 ℃ for several days until the specimen's weight remained unchanged.

As shown in Fig. S1c, five strain gauges were pasted on one of the prepared diorite specimens to investigate the basic mechanical property of the specimen. The results are illustrated in Fig. S1d. The deformations in the different regions exhibited considerable differences. The deformation of the loaded volume was significant, but no considerable strain occurred at the upper unloaded end, suggesting that the specimen was loaded partly and the upper part was approximately unstressed. In the process of loading to failure, the deformations of the side surface were nearly linear, and unstable deformations occurred several seconds before specimen failure. This result indicates that the diorite specimens were typical brittle materials. At the subsequent loading stage, the axial direction of the underside was severely compressed, and lateral deformation was released suddenly due to the unstable cracking, indicating the significant lateral expansion of the specimen. The specimen was broken suddenly and completely when the stress reached the peak stress (136 MPa), illustrating that the stress concentration effect along the press head edge was eliminated with such a loading mode.

2.2 Experiment setup

The experiment setup is shown schematically in Fig. 2. A rock specimen was placed on a platform, and its lower edge was at the same height as the press head. Conductive copper foil with a thickness of 0.06mm was pasted tightly on the rock surface to receive electric charges. The specimen was electrically isolated from the press heads and platform by thin polytetrafluoroethylene (PTFE) pads (thickness of 0.6 mm), which can also absorb machine noise. An AE sensor was bonded to the flat specimen surfaces. Before mounting the AE sensor, a transparent tape was placed on the copper foil so that the charges generated in the loaded specimen and collected by the copper foil would not be influenced by the metal AE sensor. Meanwhile, a suitable amount of Vaseline was applied between the probe and the transparent tape to enhance the reception of AE signals. Considering that electrical signals in the environment exert a substantial impact on the effective measurement of the electric currents of a loaded rock, which was often performed with slight and subtle variations in previous studies, we conducted the experiments in a closed electromagnetic shielding cage formed by red copper wire (800 meshes). Two press heads were grounded to release possible charges from the loading machine.

A servo-controlled loading machine was used to provide uniaxial compressive stress on the rock specimens. The loading machine was specially designed to deliver a maximal 500 kN axial load with precision higher than ±1%. Electric current measurements were carried out with a Keithley 3706A electrometer equipped with a multichannel scanner card (Keithley 3721ST). The measurement range was 1pA –100μA with an accuracy of 1nA. The sampling frequency of the electric signals was 33 Hz. The negative electrode of the electrometer was connected to the copper foil pasted on the lower part of a rock specimen through a coaxial cable (RG 58U), and the positive electrode was connected to the copper foil pasted on the upper part of the specimen. AE signals were detected using DS5-8A system through piezoelectric sensors (RS-2A sensors, 50 – 400 kHz). Pre-amplification of 40 dB was used and the sampling frequency of the AE signals was 3 MSPS. The threshold for the detection of an acoustic event was set to 10 mV.

The dried diorite specimens were subjected to progressive loading at a constant rate of 1 kN/s, and the time series of the electric currents and AE signals were recorded simultaneously. The experiments were conducted several times to ensure the reproducibility of the results and the validity of the derived correlations between electrical currents and external loads. After experiments, the fragments of broken rock specimen used for SEM (TESCAN mira4) were first cleaned with pure water and paint thinner, with which the greasy dirt and fine particles on the rock surface were wiped off. Then the samples were dried at 120℃ for two hours. All the specimens were coated with gold (200 thickness) prior to SEM observation in order to prevent surface charging under the SEM electron beam.

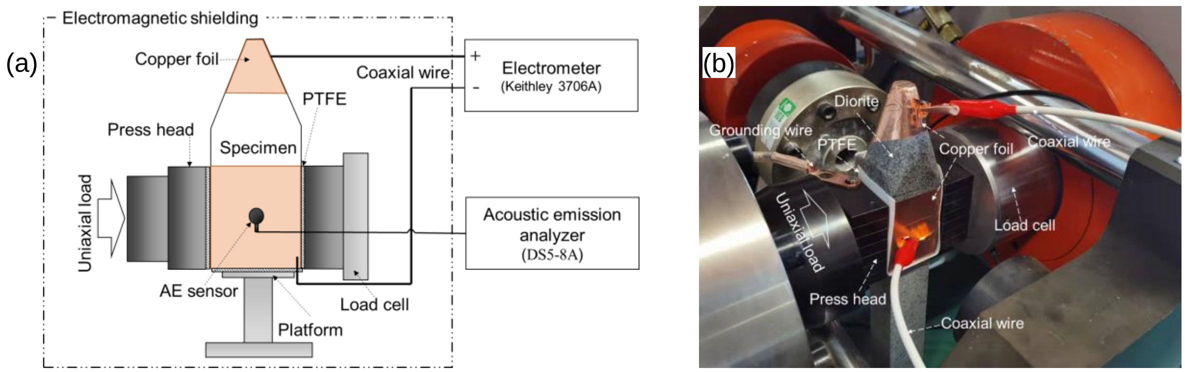

Figure 2. Experiment setup in this study. **(a)** Schematic of the experiment setup used for the measurement of PSRC and acoustic emission during uniaxial loading of diorite specimens. **(b)** Photograph of a specimen inside the load frame.

3 Results

3.1 Experimental setup and procedures

The detailed temporal variation of the PSRC flowed through specimen S1 is shown in Fig. 3a. Before the loading, PSRC was maintained at around 0 nA and showed slight fluctuations, which were caused and determined by the background noise. The load began to increase at 60 s, but no remarkable PSRC change appeared. When the load reached 396 kN at 456 s (stress level of 117.6 MPa) and equaled ~91.6% of the failure strength (σ_f = 128 MPa), a step-like increase in PSRC was measured, i.e., PSRC increased gradually from 456 s to 469 s then became steady. To express this step-like increase in PSRC clearly, the originally measured PSRC signals are smoothed and illustrated by an orange solid line in Fig. 3a. PSRC increased by 2.9 nA (ΔC_0) in the step-like increment process, after which PSRC remained at high-level values with background noise until it approached rock failure. As shown in Fig. 3b, PCS began to change dramatically and showed a sharply positive fluctuation with a huge amplitude of +114 nA at 0.48s before specimen failure. Afterward, PSRC showed a large negative fluctuation with an amplitude of -60 nA and several other fluctuations with relatively large amplitudes prior to specimen failure; this result demonstrates that the PSRC variations prior to rock failure might be determined by the complicated physical process.

The AE signals of S1, which were produced by the rapid growth of microcracks inside the rock volume, were detected simultaneously (Fig. 3a). In the beginning of loading (t = 60 s), only one AE event occurred, and it was caused by the closure of pre-existing micropores or specimen flaws. No AE occurred until 217 s, suggesting that the specimen was deformed elastically during this period. From 217 s to 310 s, microcracks began to develop, and a few scattered AE events occurred. Physically, these microcracks were isolated and discrete. Continuous, considerable AE occurred after 310 s, suggesting that the stress-induced microcracking became intense and the microcracks started to nucleate from pre-existing flaws. After 310 s the evolution of AE could be divided into three relatively separate phases with respect to the AE rate and AE energy. Each phase began with an intense AE rate and ended with a relatively high AE energy, indicating that an independent and significant fracturing process occurred inside the specimen. The silence stage between intensive AE events suggests that the rock specimen was stressed locking. Two seconds before specimen failure (Fig. 3b), AE was not measured anymore, which indicates that the specimen was in a state without microcracking but contained huge restored deformation energy for impending failure.

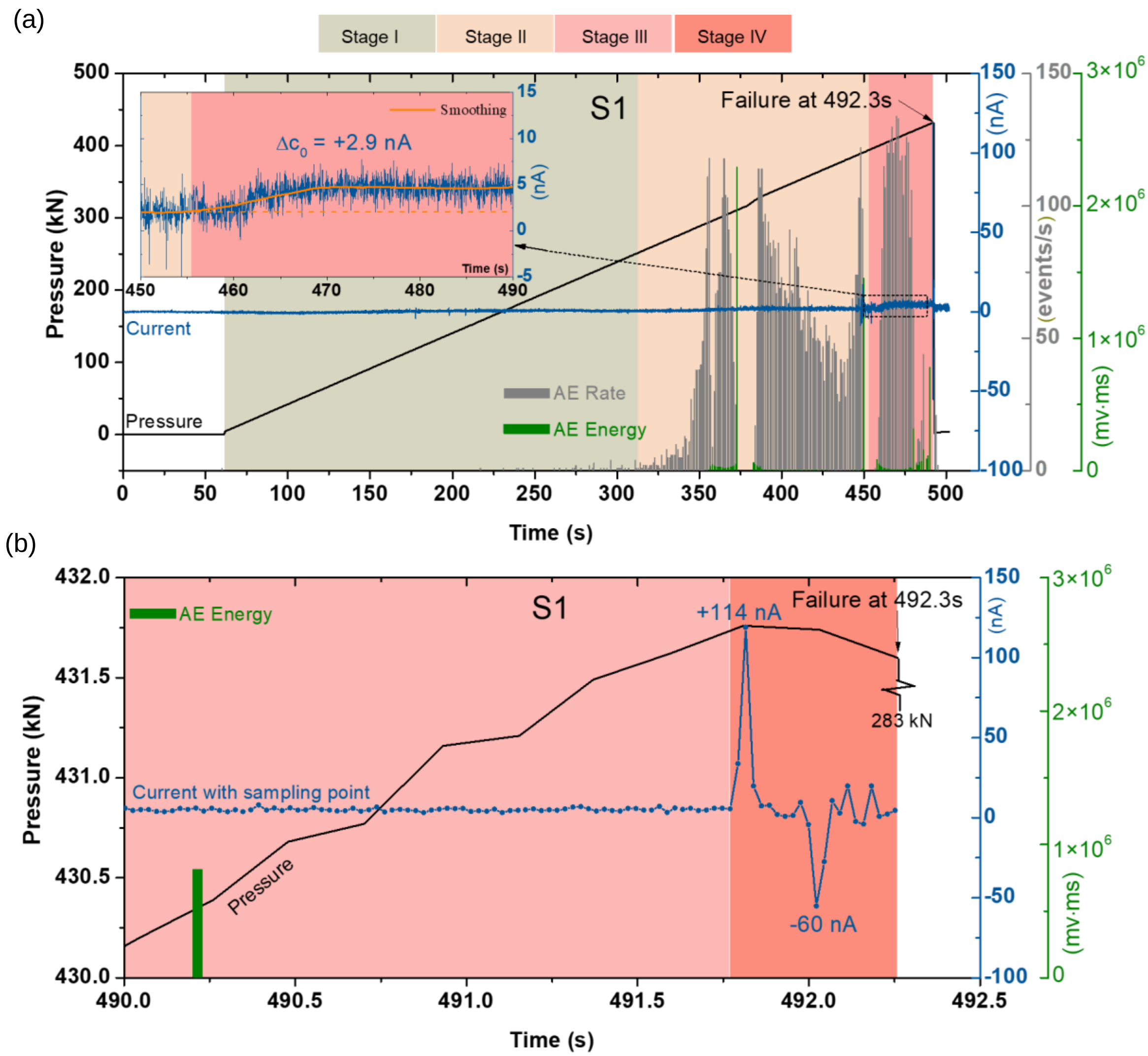

Figure 3. Detected signals in diorite specimen S1. **(a)** Signals measured during the entire loading process and **(b)** signals measured several seconds prior to specimen failure, the bule dots represent the sampling points of electric current.

Considering the relationship between the PSRC variations and evolutions of AE events in S1, we summarize the following points. First, the step-like increase in PSRC was measured at a stress level of $0.92\sigma_f$, whereas considerable AE activity was measured when the stress ratio was equal to $0.68\sigma_f$, which is much earlier than the remarkable variation in PSRC and indicates that the step-liking rise in PSRC may be related to the accumulative AE events. Second, although a huge amplitude of +114 nA and subsequent significant fluctuations were illustrated prior to rock failure, no AE signals were detected during this short period, indicating that the noteworthy PSRC variations prior to rock failure were independent of rock fracturing.

On the basis of the features of PSRC and AE measured in the experiments, the entire loading process could be divided into four characteristic stages: early silence stage (stage I), during which the PSRC and AE variations were not considerable; AE developing stage (stage II), during which AE was considerable and even intensive but no remarkable PSRC variations were shown; PSRC rising stage (stage III), during which a step-like rise in PSRC was exhibited and the accumulative AE events and AE energy exceeded 50% of their eventual values; and the final stage (stage IV), which occurred about 1 second prior to abrupt failure and where PSRC showed drastic fluctuations but AE was relatively unchanged.

Diorite specimen S1 was broken explosively, several macroscopic fractures were produced parallel to the loading direction, and finely ground rock particles were formed (Fig. 4a and 4b). The lower part of the specimen was laterally dilated by several tensile fractures under compression. Meanwhile, the measured macroscopic tension fractures and the separate fragments indicate that the loaded lower part of the specimen was broken sufficiently. The upper conical end of the specimen was not broken and remained complete, but it was separated explosively from the loaded part by 0.5–1 meter when the specimen reached failure, indicating that the energy released for rock fracturing was considerable. The formation of large fragments of the broken specimen was mainly determined by the axial–parallel fractures, and the destruction of rocks was always accompanied with the formation of separate particles (Viktorov and Kochanov, 2016), which was mainly caused by the linkage of trans-granular cracks to form detached slivers of the broken materials (Fronseak et al., 1985). To investigate the distributions of microcracks in broken S1, SEM observations were performed. The results are illustrated in Figs. 4c–4e. The micrograph of the surface of the upper part (Fig. 4c) indicates that no observable microcracks were distributed; it also suggests that the upper part of the specimen was not influenced by the applied pressure, and the original structures was approximately not changed. By contrast, on the pressed surface (Fig. 4d), a typical tensional microcrack with a width of 2–3 μm that passed across grains was measured. It displayed a characteristic Z-like shape [30], demonstrating that large amounts of microcracks were distributed on the pressed surface in addition to the observable macroscopic fractures. Moreover, the microcracks generated on the freshly fractured surface were interrelated but not sheard (Fig. 4e), and the cracks and crystal cleavages were observable, indicating that the grain-boundary and trans-granular microcracks developed well inside the loaded sub-volume of the specimen.

To ensure the reliability of the experimental results, the same tests were performed on six other diorite specimens (S2–S7). The obtained PSRC and AE signals during the loading processes and during several seconds prior to specimen failures are shown in Figs. S2 and S3, respectively. Under the progressive–compressive loading to failure, the evolutions of the PSRC of these specimens could also be divided into three phases similar manner to that of S1. Specifically, PSRC showed a relative plateau in the early loading stage, followed by a typical step-like increment when the stress level reached 0.85–0.98σ_f. Then, dramatic fluctuations with huge amplitudes occurred in the final stages of the loading process. Accordingly, the entire loading processes of these specimens could be also divided into four stages in a similar way to S1 with respect to the features of PSRC and AE. Notably, the AE activity of each diorite specimen differed. On the one hand, in the diorite specimens prepared for testing, the microscopic cracks, including grain boundary, intergranular and intragranular cracks (Simmons and Richter, 1976), were often irregular and ragged; thus, during the loading process, the microcracking induced by stress concentration (Gallagher et al., 1974; Krzna, 1979), elastic mismatching, (Wang and Heard, 1985) and twining (Olssonn and Peng,

1976) at the microscale was specific. Consequently, the time-dependent behavior of AE activity directly related to the evolution of microcracks (Atkinson, 1987) may show differences in AE rate and AE energy. On the other hand, the natural geological environment and the sampling processes of specimens differ, leading to a difference in their stress history and Kaiser effect (Kurita and Fujii, 1979).

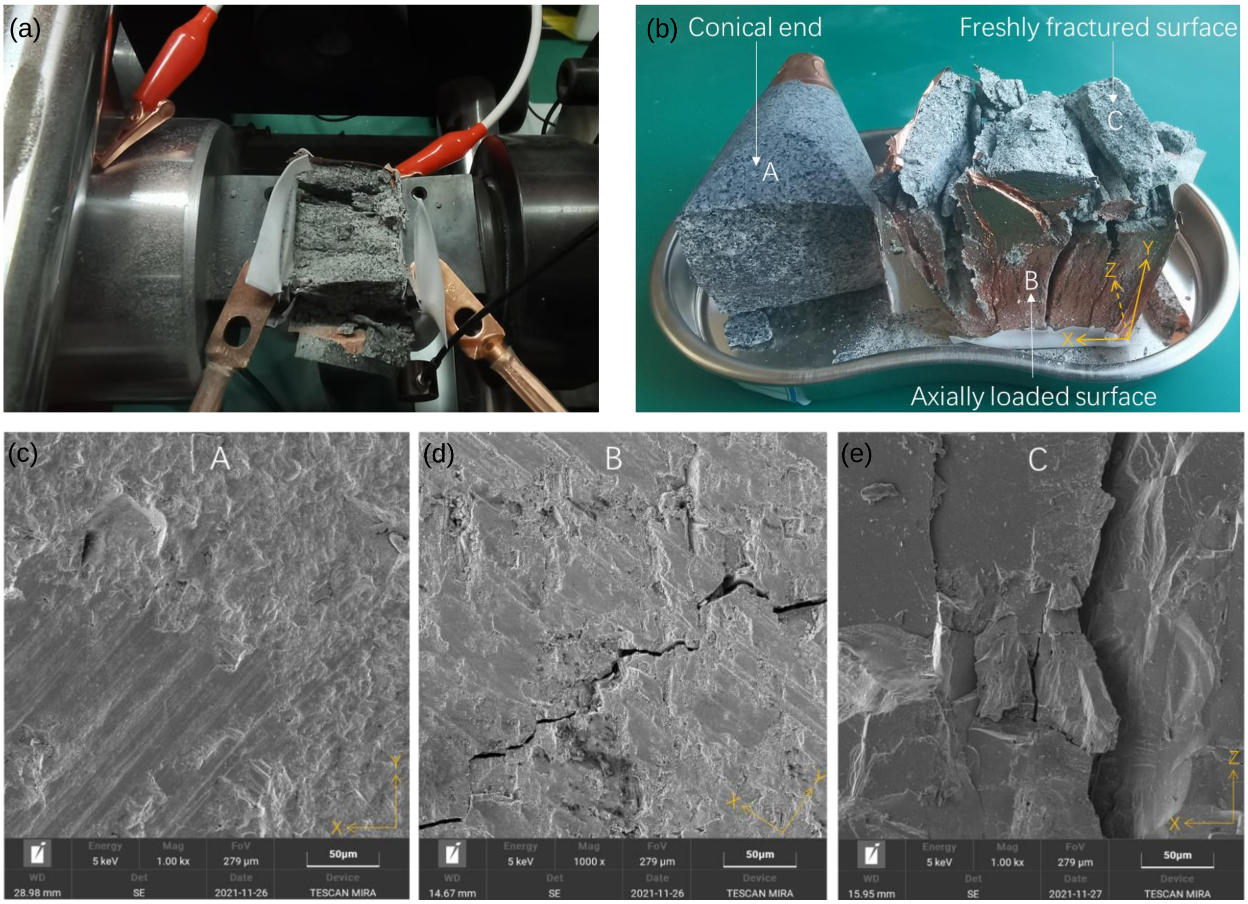

Figure 4. Photos of the broken diorite specimen S1. (a) The conical head separated explosively from the specimen as specimen failure and **(b)** front surfaces axially loaded in the experiment. **(c)-(e)** SEM micrographs of different regions on broken specimen S1. “A” illustrates the polished specimen surface at the upper part, “B” illustrates the specimen surface subjected directly to the pressure, and “C” illustrates the freshly fractured surface.

Considering the differences in the behaviors of the AE signals of the specimens, the evolutions of the AE of each specimen were normalized with respect to the total number of events and total energy (Fig. S4). The AE events of all specimens began to increase considerably when the stress level exceeded $0.65\sigma_f$, suggesting that at the early loading stage, the growth of microcracks in all specimens was slight and limited. With the further increase in applied stress, the accumulative AE events of the specimens showed different behaviors. S1, S3, and S5 presented a relatively linear tendency; S2 and S4 showed a gradual increase followed by a rapid increase, and S6 and S7 exhibited a fast–slow–fast increasing trend. Moreover, the evolutions of the accumulative AE energy of the specimens were similar despite the corresponding stress levels. Generally, three sudden increments were exhibited during the entire loading process. Considering the relationships between the step-like rise in PSRC and the applied stresses, the AE behaviors, and the strain changes (shown in Fig. 5), we derived the following conclusions. First, although the initiation of the step-like rise in PSRC corresponds to different stress levels (~0.84–0.99σ_f) for different specimens, the high stress level of loaded specimens is likely to cause a remarkable increase in PSRC. Second, if the total damage of a given specimen is certain as loading it to failure, then the accumulation of damage corresponding to at least 50% of the total number of AE events and AE energy is important for inducing significant PSRC. Third, a specimen is strengthened at the stress level of 0.85–0.99σ_f, during which the increase in stress is faster than that in strain; this might be related to the step-like rise in PSRC. Lastly, the drastic variations in PSRC prior to specimen failure might be influenced by the abnormal variations of strains at the final loading stage, where the vertical strain is released suddenly and the axial strain is increased drastically.

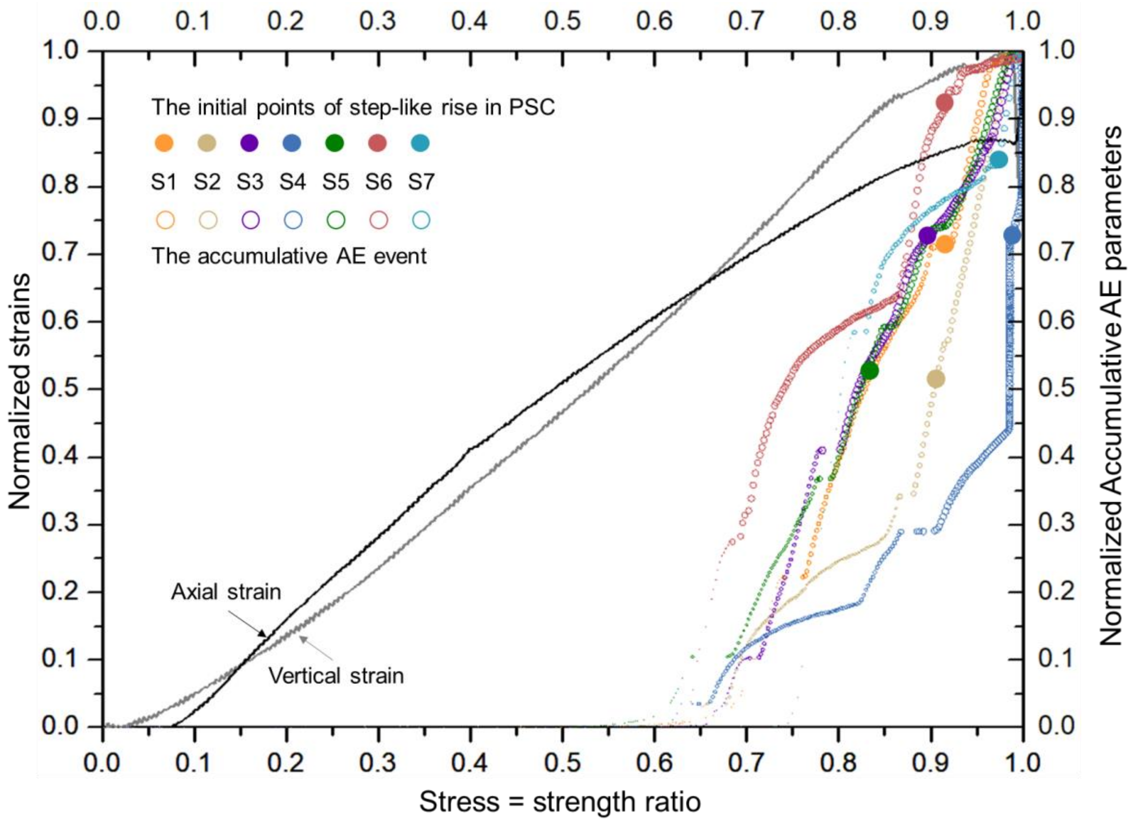

Figure 5. Relationships of the step-like rise of PSRC and the applied stress, the strains, the accumulative AE events and the accumulative AE energy. The sizes of colored circles illustrate the normalized accumulative AE energy, which behave its maximum at the moment of abrupt final failure.

Notably, the drastic fluctuations of PSRC in all specimens occurred at the very last instant just before the maximum failure stress was reached, which is generally within 1 second, and the first fluctuations were always positive (Fig. S3). This result indicates that the initiation of dramatic PSRC variations prior to rock failure might have the same physical process for different specimens, although the failure strength, PSRC variations, and development of micro-fracturing in these specimens are considerably different. Statistically, the amplitudes of the step-like rise in PSRC for all specimens in this study were 3–4 nA, and the drastic fluctuations of PSRC that occurred 1 second prior to specimen failure showed wide range of variations with respect to their amplitudes and directions. Table S1 summarizes the experimental results on the PSRC variations of all specimens.

4 Discussion

4.1 Battery effect related to PSRC variations

By applying uniaxially compressive load on the bar-shaped diorite specimen with a conical head, the diorite PSRC illustrated obvious features, as shown in Fig. 6a, including (1) step-like rise in PSRC as the accumulative damage developed to a certain degree; (2) positive fluctuation of PSRC prior to specimen failure and (3) negative fluctuation for several specimens. Before discussing the mechanism of these special PSRC variations, we need to know first what physical process these PSRC variations represent.

Generally, the variation in PSRC detected from a loaded rock specimen is a reflection of the generation and redistribution of charge carries inside rock volumes or on the rock surface. In our experiments, the negative electrode of the electrometer was connected to the copper foil pasted on the lower part of the rock specimen, and the positive electrode was connected to the copper foil pasted on the upper part of the rock specimen. Therefore, in terms of the step-like rise or positive fluctuation of PSRC, the rock specimen behaved like a battery, as shown in Fig. 6b. The upper part of the specimen served as the cathode with electrons flowing into it, and the lower part (loaded end) functioned as the anode with electrons flowing out of it. Similarly, the negative fluctuation of PSRC demonstrated that the upper part of the specimen behaved as the anode, and the lower part (loaded end) behaved as the cathode, as shown in Fig. 6c. To investigate the mechanism of the measured PSRC variations in our experiments, we determined how the applied pressure induced the differences in potential between the upper and lower parts of the diorite specimen.

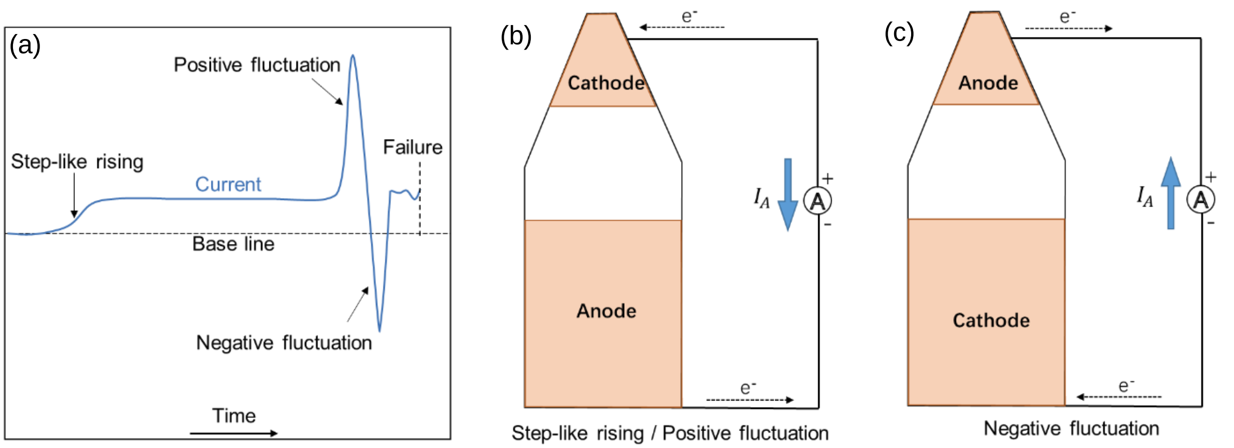

Figure 6. Schematic of the battery effect with respect to the PSRC variations measured in the experiments. (a) The typical features of PSRC revealed in out experiments. **(b)** The forward current indicates the upper part as cathode and lower part as anode, while **(c)** the reverse current indicates the exchange of specimen's electrodes.

4.2 Holistic mechanisms of PSRC from the rock specimen

Several mechanisms have been proposed to interpret the electrical signals produced by stressed rocks and minerals; these mechanisms include field emission of electrons due to crack charge separation (Enomoto and Hashimoto, 1990), piezoelectric effects (Yoshida et al., 1994), electrokinetic effects (Mizutani et al., 1976), moving charged dislocations (MCD; Slifkin, 1993; Hadjicontis and Mavromatou, 1994; Vallianatos and Tzanis, 1998), and outflow of positive holes (P-hole; Freund, 2002, 2006). The piezoelectric effect refers to the capability of the quartz mineral to generate an electric charge when rapid stress changes occur due to dynamic rupture. Given that the tested thin section of diorite (Fig. S2) illustrated that the amount of quartz minerals embodied in the tested diorite was small, we confirmed that the piezoelectric effect was not the cause, at least not the main cause, of the PSRC production in our tests. Electrokinetic phenomena are caused by the presence of an electric double layer formed at the solid–liquid interface, which means the electrokinetic effect needs the participation of liquid. However, the tested specimens in this study were air-dried several days before testing, and diorite usually has low porosity; thus, the electrokinetic effect can be ignored.

Field emission of electrons is associated with crack charge separation during rock fracturing. With the opening of a fracture in rock volume, the charges are separated on both sides of the crack, where high electric fields in the order of 10^6–10^7 V/cm are produced between the crack walls and result in the field emission of electrons (Enomoto and Hashimoto, 1990, 1992). A perfect correlation between the appearance of electric signals and the occurrence of cracking was measured and confirmed in the indentation loading experiments, and signals related to negatively charged particles (representing electrons or negative ions) and positively charged particles appeared during loading (Enomoto and Hashimoto, 1990, 1992). With the micro- and macro-fracturing of the rock specimen, the effects of crack charge separation or field emission could affect the generation and distribution of electric charges of the rock volume. However, with regard to the crack charge separation mechanism only, our experimental results revealed two controversial phenomena. First, the initiation of considerable AE events did not induce observable variations in PSRC, and AE activity did not show regular variations before and after the step-like rise in PSRC. Second, physically, if the fracture initiated inside the rock volume but did not penetrate onto the rock surface, how did crack charge separation influence the detected PSRC in our experiment? Third, the dramatic PSRC variations that occurred prior to rock failure showed poor relationships with AE activity.

The MCD mechanism always occurs in association with brittle fracturing (Vallianatos et al., 2004). In a crystalline structure, charged edge dislocation, which is electrically neutral in thermal equilibrium (Whitworth, 1975), is moved under a dynamic process and no longer maintains neutrality, thereby inducing an electric signal (Slifkin, 1993). An experimental study conducted in 1994 reported that a variation in electric signals occurs when the applied stress increases at an increasing rate, but no change in electric signal occurs when the stress increases at a constant rate (Hadjicontis and Mavromatou, 1994). Thereafter, Vallianatos et al. (2004) developed MCD theory and correlated the variation in electric currents to the changing Young's modulus. They found that PSRC only appears when the stress is high enough for the material to enter the plastic deformation phase. The MCD model is generally accepted and has been verified by many experiments on rocks and minerals (Stavrakas et al. 2004; Triantis et al. 2006; Anastasiadis et al. 2007; Stergiopoulos et al. 2015). MCD theory appears to be responsible for the step-like rise in PSRC measured in our experiments. However, providing a reasonable explanation for the potential difference between the upper and lower parts (Fig. 6) is difficult.

From a chemical point of view, peroxy defects, which are typically formed with a molecular structure of $O_3X\text{-}OO\text{-}YO_3$ (X, Y=Si^{4+}, Al^{3+} etc.), are ubiquitous in rock forming minerals of the Earth's crust (Rossman, 1996) and embodied massively in silicates (Freund et al., 2006) and igneous rocks (Freund, 2002; Balk, et al., 2009). The peroxy bond (-OO-) in rock materials can be disturbed by additional stress; as a result, positive holes are produced and propagate from the stressed rock volume to the unstressed parts (Freund et al., 2006; Scoville et al., 2015). Given that diorite is a typical igneous rock and the particular loading and detecting mode applies (Fig. 2), the effect of peroxy defects could be an underlying mechanism of the diorite PSRC measured in our experiments. Scoville et al. (2015) found that upon loading a rock with a constant rate, the current begins to rise rapidly and reaches its maximum at 5 MPa, which is far smaller than rock strength. However, such a phenomenon did not occur repeatedly in our experiments.

Physically, the experimentally detected variations in PSRC could be attributed to a combination of several mechanisms rather than a single one, and all the possible mechanisms or physical processes should be considered simultaneously. In the following parts, the contributions of different mechanisms at different stages are analyzed and discussed in detail.

4.3 Step-like rise in PSRC

4.3.1 Causes of PSRC remains indistinctive at the first two stages

Despite the effects of the loading and detection method applied in our experiments, the theories of MCD and field emission of electrons can reasonably explain why PSRC kept “silent” at stage I because no or only a few dislocations or microcracks occurred during this period. However, several studies have demonstrated that PSRC rises immediately as the specimen is loaded because the dormant -OO- embodied can be activated when the peroxy bond angle is changed (Freund et al., 2006; Scoville et al., 2015; Li et al., 2021a, 2021b). In our experiments, a remarkable rise in PSRC did not occur at the early loading stage. The mineral components of the diorite specimen, namely, plagioclase, pyroxene and biotite (Fig. S1a), are typical tectosilicate, inosilicate, phyllosilicate minerals, respectively, within which the structural units of $O_3Si\text{-}OO\text{-}SiO_3$ bearing dormant peroxy links (-OO-) are richly embodied (Freund, 2002). Therefore, as shown in Fig. 7a, the low-level pressure can also disturb the peroxy links and activate h•, which propagates through the stationary O^{2-} sublattice; their mutual electrostatic repulsion forces them to the unstressed or less-stressed surfaces. In fact, the numerical simulation results show that stress is also distributed on the upper part of specimen (Fig. S6), but the values of stress on upper part are much less than that on lower part; thus, the stress gradients along with the height of specimen was formed and the h• propagated to upper part of specimen. In such case, the upper unloaded volume of the specimen most likely behaves as the cathode due to the accumulation of h•. Accompanied with the activation of h•, the decoupling peroxy bond receives an electron (e^-) from the neighbouring $[SiO_4]^{4-}$. Freund (2006) supposed that the trapped e^- is loosely bonded and can move within the stressed rock volume. Thus, the lower pressed volume behaves as the anode. Once the connection between the upper and lower parts is established, the circuit loop closes, allowing the electrons to flow out (Fig. 7b).

For a given rock type, the amount of stress-activated h• mainly depends on the stressed volume of the rock specimen. In laboratory experiments (Freund et al., 2006) on a long granite slab, when one end (the stressing volume was about 1500 cm^3) of the slab rock was compressed at a constant rate of 0.1 MPa/s until 67 MPa, the measured PSRC increased linearly at a rate of 10.4×10^{-3} nA/s. In our experiments, the compressed diorite volume was 161.3 cm^3, and the loading rate was (0.3 MPa/s. The PSRC induced by h• is expected to be approximately 1.1×10^{-3} nA/s about. The impact of such a small amount of h• on PSRC was limited and most likely obscured by the background noise. Consequently, remarkable PSRC variations were difficult to observe at the early loading stage. Meanwhile, part of stress-activated h• could also propagate to the less-stressed side and bottom surfaces. Thus, the amount of net negative charges that could be received by the lower copper foil was smaller than the amount of h• flowing into the upper copper foil. The induced PSRC variation was limited because the electric current flowing through the closed circuit was physically determined by the relatively small amounts of net negative charges flowing out from the lower part.

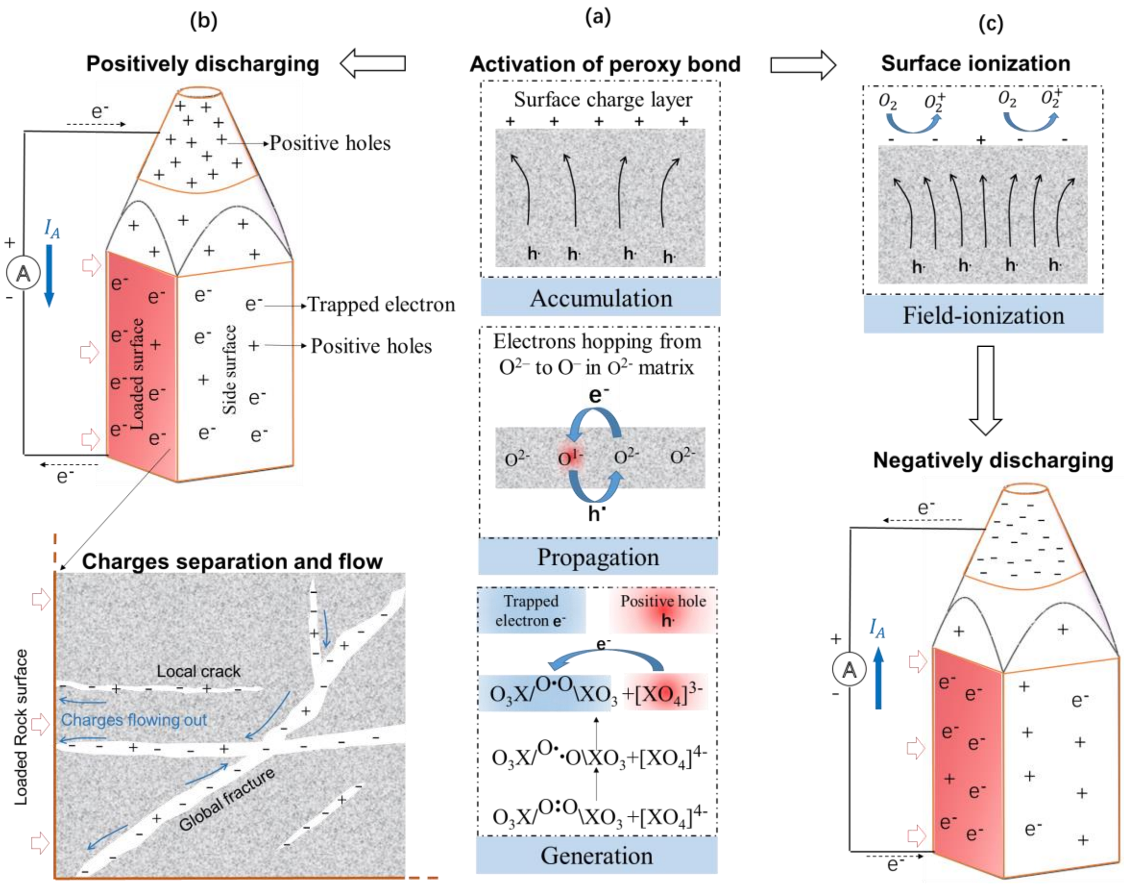

Figure 7. Stress-activated positive hole charge carries in the partly loaded diorite specimen. (a) Generation and propagation of positive hole charge carries, **(b)** positively discharging effect, and the local cracks and global fractures in the lower part of specimen, **(c)** negatively discharging effect induced by surface ionization.

With the increase in compressive stress, the AE activities began to occur when the stress exceeded $0.6\sigma_f$. At stage II, the microcracks initiated from local stress concentrations resulting from mismatches in elastic properties along the grain boundaries (Tapponnier and Brace, 1976) or from natural flaws and pores (Sprunt and Brace, 1974); thus, these microcracks were distributed discretely as local cracks (Fig. 7b, Fig. S7). As shown in Fig. S8, in the process of fracturing the peroxy bond embedded in the crack tip would be bent and decoupled, then separated thoroughly. It is no doubt that h• would be released in the process of bending, and an extra electron would be trapped at the parent peroxy entities at the same time. With the complete separation of the bond, the previously trapped electron would occupy the valence band of oxygen as an eight-electron configuration and become immobile. At the same time, the other unpaired electron behaves as dangling bond, that are expected to trap the free electrons on or near the freshly created crack wall surface, i.e., the negative charges separated on the crack walls may be consumed by such dangling bond (Dickinson et al., 1981). Only when local cracks are generated on or in the vicinity of a specimen surface, the micro-fracturing induced charges, including crack separation charges and electrons driven by field emission (Enomoto and Hashimoto, 1990, 1992), could be transferred to the copper foil, and the total net electrons flowing out the lower part may increase accordingly. However, our numerical simulation results show that most of the newly generated microcracks at early loading stage (before $0.85\sigma_f$) were inside the rock volume rather than on the rock surface (Fig. S7), and notably these local cracks are discrete and isolated; thus, their negative charges could not be transferred to the rock specimen surface at stage II. Therefore, with the comprehensive effects of the reduction in loosely trapped electrons at the parent peroxy entities and the slight increase in negative charges from the rock surface cracks, the PSRC variation was still indistinctive.

The above-mentioned MCD mechanism is also associated with micro-fracturing. According to MCD theory, the transient electric variation of a crystalline structure in a dynamic process is related to the non-stationary accumulation of deformations (Vallianatos et al., 2004). When the stress exceeds the elastic limit and micro-cracks begin to generate, actually the rock is still nearly linear if the micro-fracturing activity is very low (Scholz, 1968); thus, PSRC is still not changed. In addition, as illustrated in previous experiments (Stavrakas et al., 2004; Pasiou and Triantis, 2017; Li et al., 2021b), the measured currents start to increase after a certain critical stress threshold, but the maximal variations of currents could reach 0.1–0.4 nA, which is much less than the background noise of PSRC in our experiment. Meanwhile, if a crack open inside the stressed rock volume, its impact on the electric signals on the rock surface is limited because the intensity of the electric field decays with distance. Therefore, although the field emission of electrons is truly existed at stage-II in the current study, its effects on PSRC were minimal and limited.

4.3.2 Coalescence and connection of microcracks induce remarkable PSRC variations

The step-like rise of PSRC in all the specimens started at the stress level of 0.84–0.99σ_f and significant cumulative damages were reached (Fig. 5). Hence, we analyzed the characters of stage III with respect to the microstructures and charge distributions of the specimens. Physically, as the compressive loading increased further, many new microcracks are activated, and the existing microcracks continued growing until the size and numbers of the cracks were so large that they began to interfere and interact with each other, eventually linking the surface and inner cracks and forming global fractures (Fig. 7b), which are characteristic of rock specimens approaching failure [35]. We could not investigate the source locations of the microcracks by using one AE sensor only, but the numerical simulation indicates that the evolution of microcracks inside the specimen underwent coalescing and connecting processes at this stage (Fig. S7).

In fact, as illustrated in Fig. 7b, in the process of loading diorite specimen several local cracks initiated on the rock surface, during which the electric charges resulting from broken peroxy bonds or charge separations could transfer and flow into the copper foil on the surface. Meanwhile, other local cracks initiated in the inner part of the rock volume; in this case, the free electric charges formed with crack growth were constrained on or near the crack surface or crack tips until these local cracks extended to the specimen surface. In addition, the generation of global fractures at stage III attached to the specimen surface provided channels for the free charges from other local cracks inside the rock volume. On the other hand, at stage III the positive holes were also activated by the cracking behavior and propagated continuously into the upper part. Therefore, with the coalescence and connection of the microcracks, abundant cracking-induced negative charges were transferred to the rock surface and led to the significant increment in PSRC.

These discussions suggest that in process of loading the diorite specimen to failure, P-hole activation, crack charge separation, and field emission were facilitated by the coalescence and connection of microcracks at a high level of stress. Notably, the critical stress level and accumulative damage may be influenced strongly by rock types, loading modes, specimen size, and the rock volume subjected to compressive load. These factors will be studied in another work.

4.4 Drastic PSRC oscillation prior to rock failure

All of the seven diorite specimens showed that drastic PSRC variations occurred one second about prior to rock failure. The physical processes prior to rock failure, especially within such a short period, are difficult to be illustrated clearly because of the impending sudden failure of diorite specimens, and the corresponding fracture mechanics or stress state in the rock volume are also poorly understood. As discussed in Section 4.3, at stage III, the intensive local cracks should have interfered and interacted with each other and developed into multiple groups of global fractures (Atkinson, 1987), which could be distributed throughout the entire rock volume. Thus, assuming that the generation of positive holes at stage III is only related to the opening of local cracks, the amounts of electrons or negative ions at the lower part that result from the broken peroxy bond, charge separations, field emission effect, and MCD effect are much larger than the amounts of positive charges transmitting into the upper part, which results only from the activation of positive holes. Hence, the detected PSRC in this study was determined by the amounts of positive holes at stage III that were kept relatively stable because the generation and consuming rates of positive holes may have a dynamic equilibrium state. As stage IV approached, a few AE signals were detected, and the significant deformation of the specimen was mainly caused by the dislocations or deformations of the lattice inside the mineral grains rather than the growth of microcracks along the grain boundary. Thus, the main generation mechanism of positive holes was changed, and the peroxy bonds embedded inside the mineral grains, the amount of which was much larger than that of the peroxy bonds embedded in the grain boundaries or flaws, might have been activated. PSRC increased drastically when the large amounts of positive holes propagated into the upper part.

At stage IV, because almost no local cracks or global fractures occurred accompanying the drastic PSRC variations, the electrons or negative ions reserved in the lower part at stage III were consumed rapidly by the large amounts of upward positive holes. Thus, the detected PSRC returned to zero instantaneously, and a positive fluctuation occurred. Most of the time, large amounts of positive holes accumulated in the upper part. The accumulation of positive hole charge carriers h• on the surface produced a positive surface charge layer, as shown in Fig. 7c, and the microscopic high electric field on the rock surface may have caused air molecules to be ionized. The field ionization of air molecules ($O_2 \rightarrow O_2^+ + e^-$) produced O_2^+ ions and electrons. At stage IV, the applied stress on the lower part might be concentrated locally because the structure of this sub-volume was changed by the multiple global fractures. Consequently, part of the sub-volume became less stressed or unstressed (Fig. S6), and the positive holes were transmitted to the surface. Therefore, as illustrated in Fig. 7c, the battery polarity was reversed; the upper part became the cathode due to the ionization electrons, and the lower part became the anode due to the accumulation of positive holes, leading to the negative fluctuation of the detected PSRC. Meanwhile, the physical processes of several positive or negative fluctuations in certain specimens are difficult to illustrate clearly because the structures, deformations, and stress concentrations at such a short stage are complex and often transient. Basically, the significant and abnormal variations of PSRC were contributed comprehensively by the physical processes mentioned and discussed above.

5 Conclusions

By uniaxially compressing cubic- and conical-shaped diorite specimens to failure and pasting copper foil on large parts of the rock surface for the first time, this study synchronously measured the pressure-stimulated rock current (PSRC) and acoustic emission (AE). The experimental results revealed that the temporal variation of the PSRC of the diorite specimen could be divided into three phases: (1) indistinctive at stages of elastic deformation and early micro-fracturing, (2) step-like rise at a high level of stress and significant accumulated damage, and (3) dramatic oscillation shortly prior to impending rock failure.

The stress-activated P-hole activation, crack charge separation, and field emission of electrons are suggested responsible for the PSRC variations, and the prominent mechanism might be different in varied phases of the PSRC evolution. The coalescence of local microcracks and its connection to global fractures provided important channels for the movement of electric charges and consequently promoted remarkable PSRC variations. The experimental results of this study provide a new understanding of the stress-activated electric current of compressively loaded rocks embodied with peroxy minerals, which exhibit potential use of dynamic signal detection of PSRC and possible precursor identification of rock fracturing, which includes but not limited to rock mass breaking, rock structure failure, mine burst, and seismic activity.

Acknowledgments

This research was supported by the Key Program of National Nature Science Foundation of China (41930108), National Nature Science Foundation of China (42101394), Project funded by China Postdoctoral Science Foundation (2021M693550)

References

1. Anastasiadis, C. , Triantis, D. , Hogarth, C. A. (2007). Comments on the phenomena underlying pressure stimulated currents in dielectric rock materials. *Journal of Materials Science*, 42(8), 2538-2542.
2. Atkinson, B. K. (1987). *Fracture mechanics of rock*. Amsterdam, The Kingdom of the Netherlands: Elsevier.
3. Balk, M. , Bose, M. , Ertem, G. , Rogoff, D. A. , Rothschild, L. J. , & Freund, F. T. (2009). Oxidation of water to hydrogen peroxide at the rock–water interface due to stress-activated electric currents in rocks. *Earth and Planetary Science Letters*, 283(1-4), 87-92. https://doi.org/10.1016/j.epsl.2009.03.044
4. Dickinson, J. T. , Donaldson, E. E. , & Park, M. K. (1981). The emission of electrons and positive ions from fracture of materials. *Journal of Materials Science*, 16, 2897-2908. https://doi.org/10.1007/BF00552976
5. Enomoto, Y. , & Hashimoto, H. (1990). Emission of charged particles from indentation fracture of rocks. *Nature*, 346, 641-643. https://doi.org/10.1038/346641a0
6. Enomoto, Y. , & Hashimoto, H. (1992). Transient electrical activity accompanying rock under indentation loading. *Tectonophysics*, 211, 337-344. https://doi.org/10.1016/0040-1951(92)90069-I
7. Fonseka, G., Murrell, S. , & Barnes, P. (1985). Scanning electron microscope and acoustic emission studies of crack development in rocks. *International Journal of Rock Mechanics and Mining Sciences & Geomechanics Abstracts*, 55, 273-289. https://doi.org/10.1016/0148-9062(85)92060-1
8. Freund, F. T. (2002). Charge generation and propagation in igneous rocks. Journal of Geodynamics, 33(4-5), 543-570. https://doi.org/10.1016/S0264-3707(02)00015-7

9. Freund, F. T. (2009). Stress-activated positive hole charge carriers in rocks and the generation of pre-earthquake signal. *Electromagnetic phenomena associated with earthquakes*, 41-96.
10. Freund, F. T. , Takeuchi, A. , Lau, B. W. (2006). Electric currents streaming out of stressed igneous rocks–A step towards understanding pre-earthquake low frequency EM emissions. *Physical and Chemistry of the Earth, Parts A/B/C*, 31, 4-9. https://doi.org/10.1016/j.pce.2006.02.027
11. Gallagher Jr, J. J. , Friedman, M. , Handin, J. , & Sowers, G. M. (1974). Experimental studies relating to microfracture in sandstone. *Tectonophysics*, 21(3), 203-247. https://doi.org/10.1016/0040-1951(74)90053-5
12. Hadjicontis, V. , & Mavromatou, C. (1994). Transient electric signals prior to rock failure under uniaxial compression. *Geophysical Research Letters*, 21(16), 1687-1690. https://doi.org/10.1029/94GL00694
13. Hoenig, S. A. (1979). Aerosol anomalies preceding earthquakes. *Nature*, 279, 169-169. https://doi.org/10.1038/276606a0
14. Kurita, K. , & Fujii, N. (2013). Stress memory of crystalline rocks in acoustic emission. *Geophysical Research Letters*, 6(1), 9-12. https://doi.org/10.1029/GL006i001p00009
15. Li, D. X. , Wang, E. Y. , Ju, Y. Q. , & Wang, D. M. (2021a). Laboratory investigations of a new method using pressure stimulated currents to monitor concentrated stress variations in coal. *Natural Resources Research*, 30, 707-724. https://doi.org/10.1007/s11053-020-09749-6
16. Li, D. X. , Wang, E. Y. , Li, Z. H. , Ju, Y. Q. , Wang, D. M., & Wang, X. Y. (2021b). Experimental investigations of pressure stimulated currents from stressed sandstone used as precursors to rock fracture. *International Journal of Rock Mechanics and Mining Sciences*, 145. https://doi.org/10.1016/j.ijrmms.2021.104841
17. Li, M. , Wang, H. T. , Wang, D. M. , Shao, Z. L. (2020). Experimental study on characteristics of surface potential and current induced by stress on coal mine sandstone roof. *Engineering Geology*, 266. https://doi.org/10.1016/j.enggeo.2019.105468
18. Li, Z. , Wang, E. , & He, M. (2015). Laboratory studies of electric current generated during fracture of coal and rock in rock burst coal mine. *Journal of Mining*, 2015. http://dx.doi.org/10.1155/2015/235636
19. Liao, C. T. , Zhang, C. S. , Wu, M. L. , Ma, Y. S. , & Ou, M. Y. (2003). Stress change near the Kunlun fault before and after the Ms 8.1 Kunlun earthquake. *Geophysical research letters*, 30(20). https://doi.org/10.1029/2003GL018106
20. Meng, W. , Chen, Q. C. , Zhao, Z. , Wu, M. L. , Qin, X. H. , & Zhang, C. Y. (2015). Characteristics and implications of the stress state in the Longmen Shan fault zone, eastern margin of the Tibetan plateau. *Tectonophysics*, 656, 1-19. https://doi.org/10.1016/j.tecto.2015.04.010
21. Mizutani, H. , Ishido, T. , Yokokura, T. , & Ohnishi, S. (1976). Electrokinetic phenomena associated with earthquakes. *Geophysical Research Letters*, 3(7), 365-368. https://doi.org/10.1029/GL003i007p00365
22. Olsson, W. A. , & Peng, S. S. (1976). Microcrack nucleation in marble. *International Journal of Rock Mechanics and Mining Sciences & Geomechanics Abstracts*, 13, 53-59. https://doi.org/10.1016/0148-9062(76)90704-X
23. Pasiou, E. D. , & Triantis, D. (2017). Correlation between the electric and acoustic signals emitted during compression of brittle materials. *Frattura ed Integrità Strutturale*, 11, 41-51. https://doi.org/10.3221/IGF-ESIS.40.04
24. Rossman, G. R. (1996). Studies of OH in nominally anhydrous minerals. *Physics and Chemistry of Minerals*, 23, 299-304. https://doi.org/10.1007/BF00207777
25. Saltas, V. , Vallianatos, F. , Triantis, D. , Stavrakas, I. (2018). Complexity in laboratory seismology: From electrical and acoustic emissions to fracture. *Complexity of seismic time series*(pp. 239-273). Amsterdam, The Kingdom of the Netherlands: Elsevier.
26. Scholz, C. H. (1968). Microfracturing and the inelastic deformation of rock in compression. *Journal of Geophysical Research*, 73(4), 1417-1432. https://doi.org/10.1029/JB073i004p01417

27. Scoville, J. , Sornette, J. , & Freund, F. T. (2015). Paradox of peroxy defects and positive holes in rocks Part II: Outflow of electric currents from stressed rocks. *Journal of Asian Earth Sciences*, 114, 338-351. https://doi.org/10.1016/j.jseaes.2015.04.016
28. Simons, G. , & Richter, D. (1976). *The physics and chemistry of minerals and rocks*. State of New Jersey, the United States of America: Wiley-Interscience.
29. Slifkin, L. (1993). Seismic electric signals from displacement of charged dislocations. *Tectonophysics*, 224(1-3), 149-152. https://doi.org/10.1016/0040-1951(93)90066-S
30. Sprunt, E. S. , & Brace, W. F. (1974). Direct observation of microcavities in crystalline rocks. *International Journal of Rock Mechanics and Mining Sciences & Geomechanics Abstracts*, 11, 139-150. https://doi.org/10.1016/0148-9062(74)92874-5
31. Stavrakas, I. , Triantis, D. , Agioutantis, Z. , Maurigiannakis, S. , Saltas, V. , Vallianatos, F. , & Clarke, M. (2004). Pressure stimulated currents in rocks and their correlation with mechanical properties. *Natural Hazards and Earth System*, 4, 563-567. https://doi.org/10.5194/nhess-4-563-2004
32. Stergiopoulos, C. , Stavrakas, I. , Hloupis, G. , Triantis, D. , & Vallianatos, F. (2013). Electrical and acoustic emissions in cement mortar beams subjected to mechanical loading up to fracture. *Engineering Failure Analysis*, 35, 454-461. https://doi.org/10.1016/j.engfailanal.2013.04.015
33. Tapponnier, P. , & Brace, W. F. (1976). Development of stress-induced microcracks in Westerly granite. *International Journal of Rock Mechanics and Mining Sciences & Geomechanics Abstracts*, 13, 103-112. https://doi.org/10.1016/0148-9062(76)91937-9
34. Triantis, D. , Stavrakas, I. , Anastasiadis, C. , Kyriazopoulos, A. , & Vallianatos, F. (2006). An analysis of pressure stimulated currents (psc), in marble samples under mechanical stress. *Physical and Chemistry of the Earth, Parts A/B/C*, 31, 4-9. https://doi.org/10.1016/j.pce.2006.02.018
35. Triantis, D. , Stavrakas, I. , Kyriazopoulos, A. , Hloupis, G. , & Agioutantis, Z. (2012). Pressure stimulated electrical emissions from cement mortar used as failure predictors. *International Journal of Fracture*, 175, 53-61. https://doi.org/10.1007/s10704-012-9701-7
36. Uyeda, S. , Hayakawa, M. , & Nagao, T. (2002). Electric and magnetic phenomena observed before the volcano-seismic activity in 2000 in the Izu island region, Japan. *Proceedings of the national academy of seicences of the United States of America*, 99 (11), 7352-7355. https://doi.org/10.1073/pnas.072208499
37. Vallianatos, F. , & Tzanis, A. (1998). Electric current generation associated with the deformation rate of a solid: preseismic and coseismic signals. *Physical and Chemistry of the Earth*, 23(9-10), 933-938. https://doi.org/10.1016/S0079-1946(98)00122-0
38. Vallianatos, F. , Triantis, D. , Tzanis, A. , Anastasiadis, C. , & Stavrakas, L. (2004). *Physics and Chemistry of the Earth, Parts A/B/C*, 29(4-9), 339-351. https://doi.org/10.1016/j.pce.2003.12.003
39. Viktorov, S. , & Kochanov, N. (2016). Experimental regularities in formation of submicron particles under rock failure. *Journal of Mining Science*, 52, 899-905. https://doi.org/10.1134/S1062739116041370
40. Wang, H. F. , & Heard, H. C. (1985). Prediction of elastic moduli via crack density in pressurized and thermally stressed rock. *Journal of Geophysical Research: Solid Earth*, 90(B12), 10342-10350. https://doi.org/10.1029/JB090iB12p10342
41. Warwick, J. W. , Stoker, C. , & Meyer, T. R. (1982). Radio emission associated with rock fracture: possible application to the great Chilean earthquake of May 22, 1960. *Journal of Geophysical Research: Solid Earth*, 87(B4), 2851-2859. https://doi.org/10.1029/JB087iB04p02851
42. Whitworth, R. W. (1975). Charged dislocations in ionic crystals. *Advances in Physics*, 24, 203-204. https://doi.org/10.1080/00018737500101401
43. Yoshida, S. , Clint, O. C. , & Sammonds, P. R. (1998). Electric potential changes prior to shear fracture in dry and saturated rocks. *Geophysical Research Letters*, 25(10), 1577-1580. https://doi.org/10.1029/98GL01222

44. Yoshida, S. , Uyeshima, M. , & Nakatani, M. (1997). Electric potential changes associated with slip failure of granite: preseismic and coseismic signals. *Journal of Geophysical Research: Solid Earth*, 1021(B7), 14883-14897. https://doi.org/10.1029/97JB00729 .

[JOURNAL OF GEOPHYSICAL RESEARCH-SOLID EARTH]

Supporting Information for

Pressure-Stimulated Rock Current as Loading Diorite to Failure: Particular Variation and Holistic Mechanisms

Wenfei Mao[1,2], Lixin Wu1[,2*], Youyou Xu[1,2], Rubing Yao[1,2], Jingchen Lu[1,2], Licheng Sun[3], and Yuan Qi[1,2]

[1] School of Geoscience and Info-Physics, Central South University, Changsha, 410083, China.
[2] Laboratory of Geo-Hazards Perception, Cognition and Predication, Central South University, Changsha, 410083, China.
[3] School of Resource and Safety Engineering, Central South University, Changsha, 410083, China.

Contents of this file

Text S1.

Simulation of stress distribution and microcracks growth. The Grain-Based Discrete Element Modelling (GB-DEM) method [1] was used to simulate the initiation and growth of microcracks in the process of loading the diorite specimen to failure by using the programs PFC2D. First, as shown in Fig. S5a, the initial two-dimensional grain structure model was created according to the contents and sizes of four main minerals embedded in diorite specimen (Fig. S1, Table S2), and the generated disks has been divided into four groups accordingly. By connecting the centers of the disks that share the same contact points, multiple convex polygons are formed correspondingly (black solid lines). Second, the centroids of convex polygons were calculated and illustrated by the red dots in Fig. S5b. Third, by connecting the red dots of polygons that share the same edge (blue solid lines in Fig. S5c), a new polygonal mesh was formed (yellow solid lines). Then, all of the original disks in the initial model were deleted and the remaining convex polygons corresponds to the mineral grains (Fig. S5d). Lastly, each newly formed convex polygon was filled with new disks, of which the scale is much smaller than that of polygon; thereby, the geometric model with polygon grain structure reflects the distributions of different mineral crystals (Fig. S5e and 5f). There are no gaps between polygons - each polygon edge is either internal (adjacent to two polygons) or external (adjacent to one polygon) such that each polygon and internal edge correspond with a grain and a grain-grain interface, respectively.

Based on the modulus and Poisson's ratio of minerals given in Table S1, "trial and error" method was used for calibrating the mechanical parameters of the filled small disks in Fig. S5e, such that the established numerical model matches the macroscopic response and most of the mechanisms that occur during compression test on diorite specimen. Besides, material properties are associated with the grains and the interfaces such that both entities are deformable and capable of fracturing. The calibrated results are listed in Table S3. The overall macro-properties of simulations and experiments are well agreed.

Type or paste text here. This should be additional explanatory text, such as: extended descriptions of results, full details of models, extended lists of acknowledgements etc. It should not be additional discussion, analysis, interpretation or critique. It should not be an additional scientific experiment or paper.

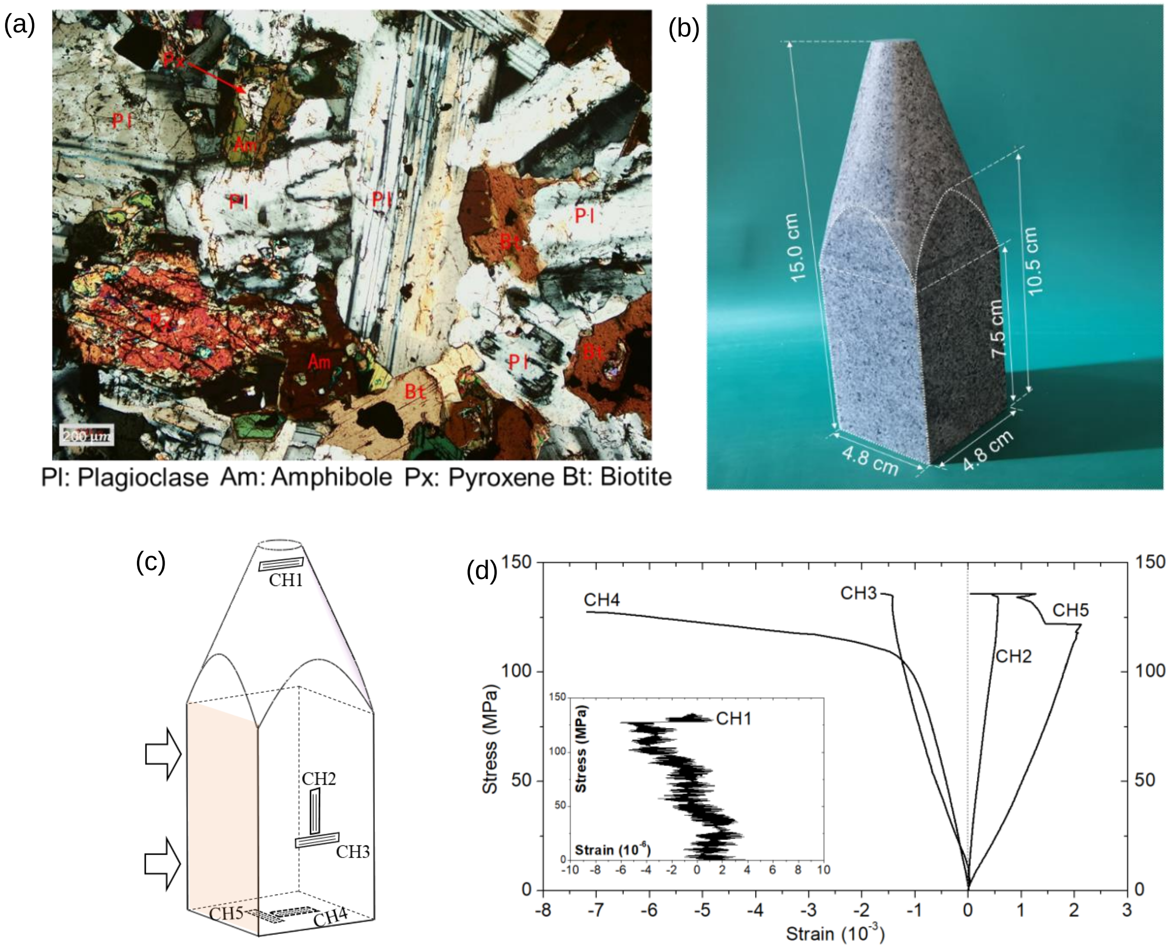

Figure S1. Preparation of rock specimen. **(a)** thin section of diorite with cross light **(b)** bar-shaped diorite specimen with a conical head **(c)** the strain gauges pasted on the specimen surface, CH2 and CH3 are pasted on side surface, CH4 and CH5 are pasted on underside surface. **(d)** the stress-strain curves of specimen in process of axially loading to failure.

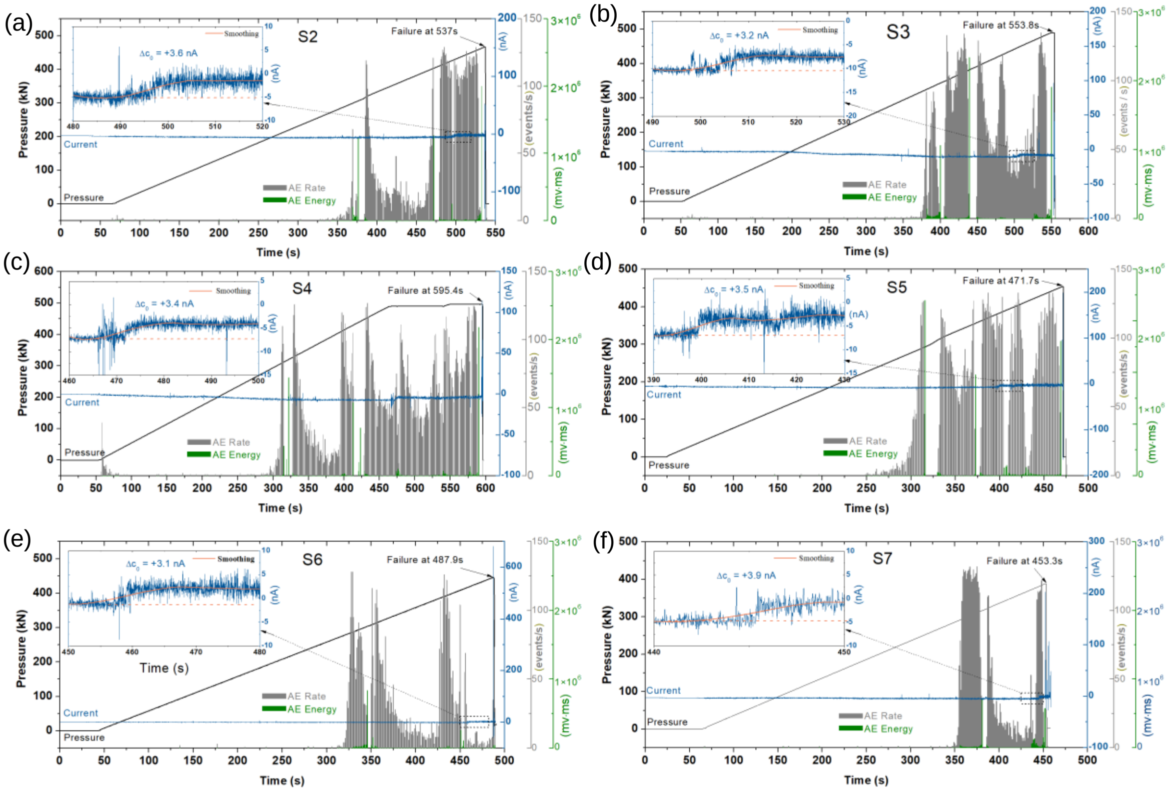

Figure S2. Detected PSRC and AE signals of diorite specimens S2 - S7, corresponding **(a) - (f)** respectively.

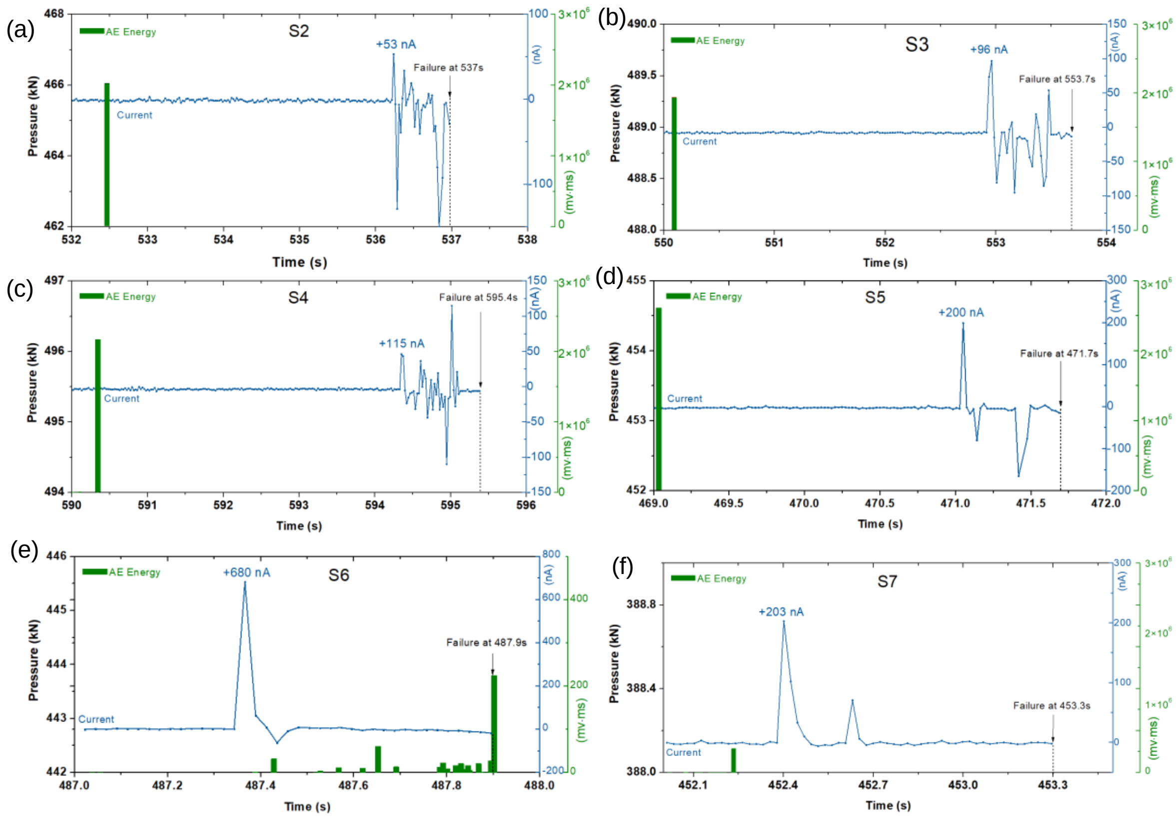

Figure S3. PSRC variations during several seconds prior to the rock failure for specimens S2-S7, corresponding **(a) - (e)** respectively.

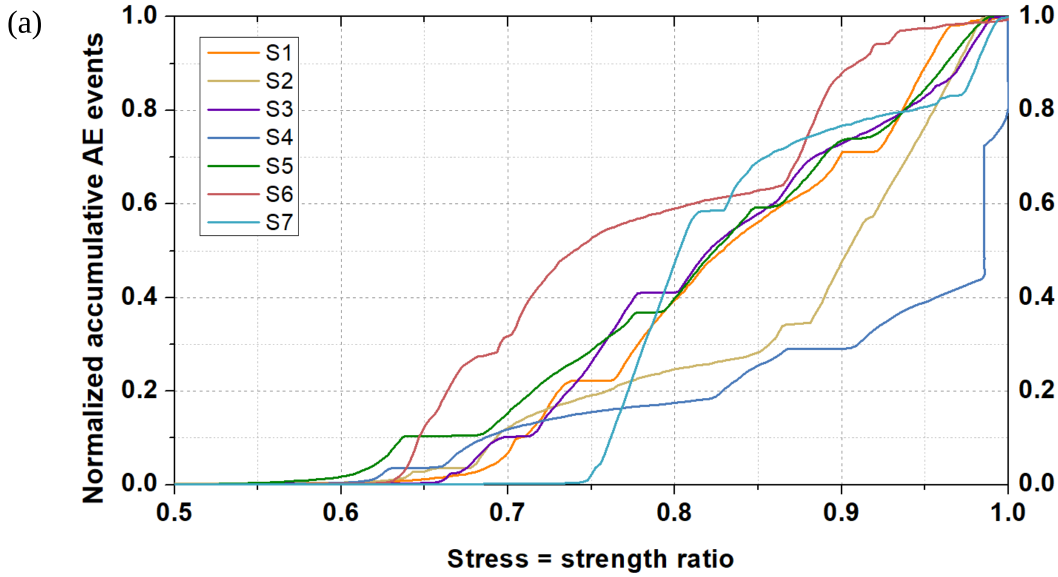

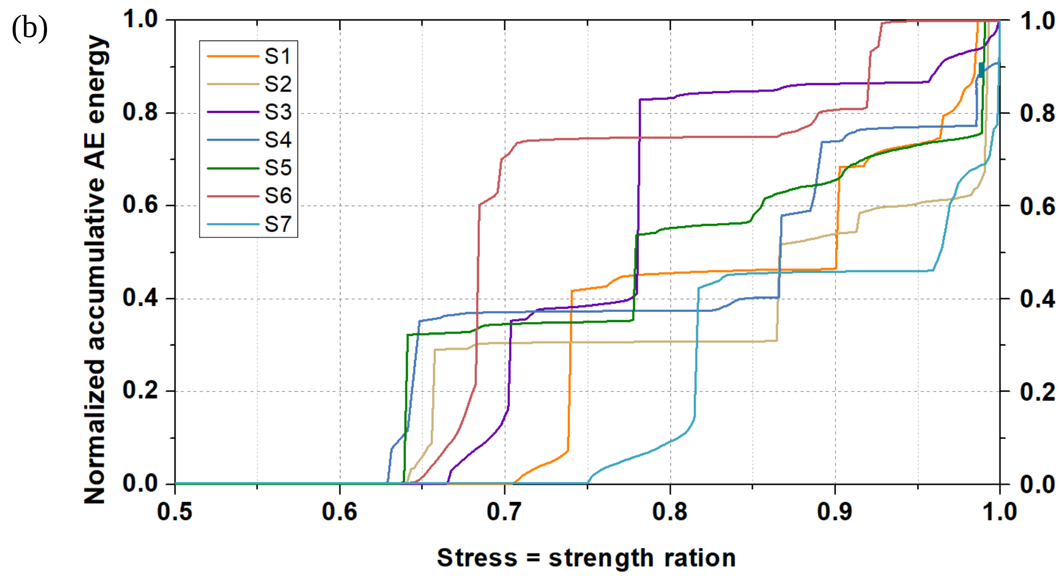

Figure S4. Relationships between the applied stress and **(a)** the accumulative AE events and **(b)** the accumulative AE energy

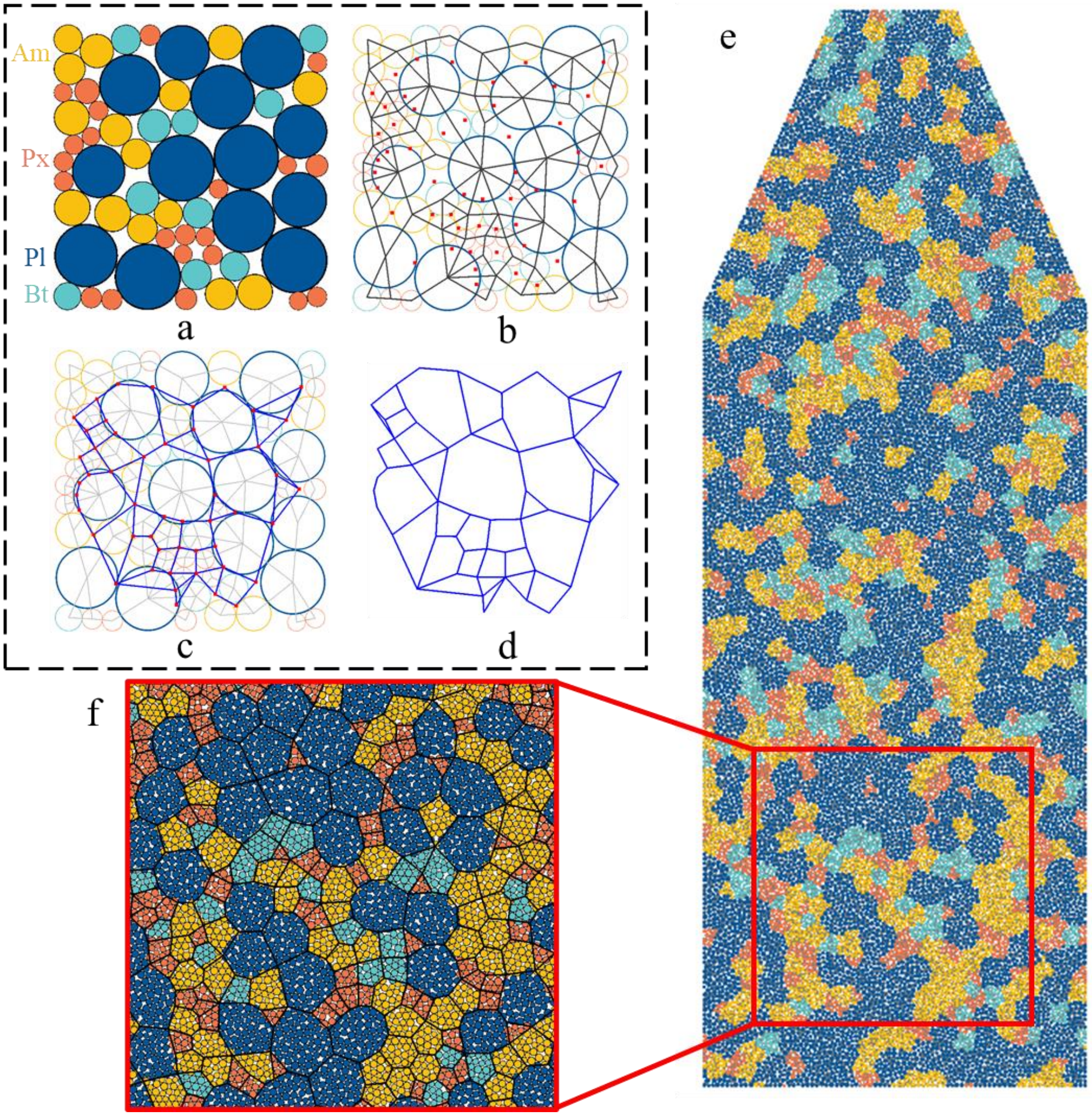

Figure S5. Construction process of grain-based discrete element method (GB-DEM). **a**. initial disk packing showing disks and contacts, where Am, Px, Pl and Bt represent four main minerals in diorite specimen that illustrated in Fig. S1. **b**. filled dots (red) at internal-void centroids. **c**. grain structure consisting of polygons, one for each internal disk, with nodes at internal-void centroids. **d**. generated polygon mesh. **e**. two-dimensional numerical model of diorite specimen in our experiment. f, enlarged polygon mesh with filled particles.

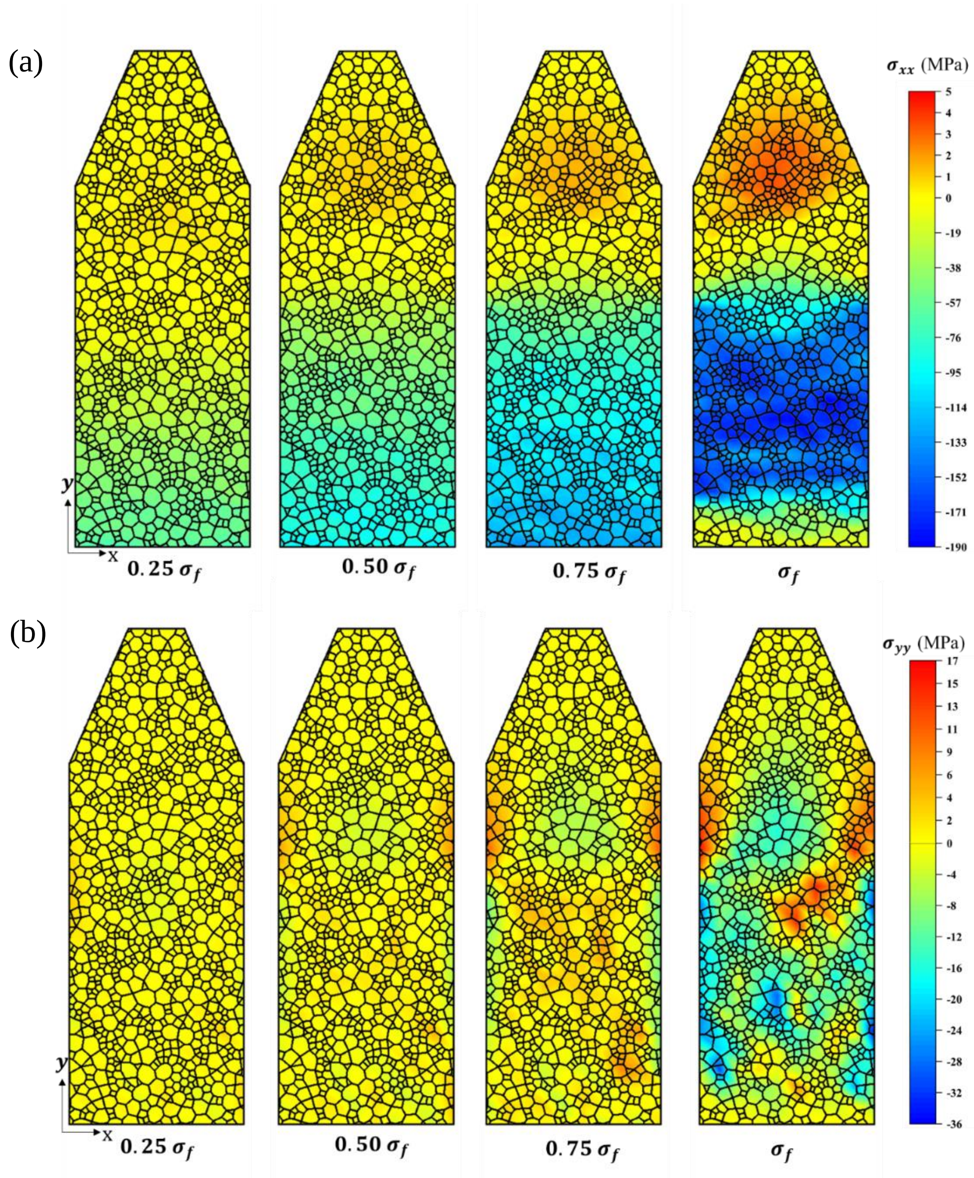

Figure S6. Results of numerical simulation (with particle flow model) for the distribution of stresses in the loaded diorite specimen. **(a)** the stress distribution at x direction; **(b)** the stress distribution at y direction.

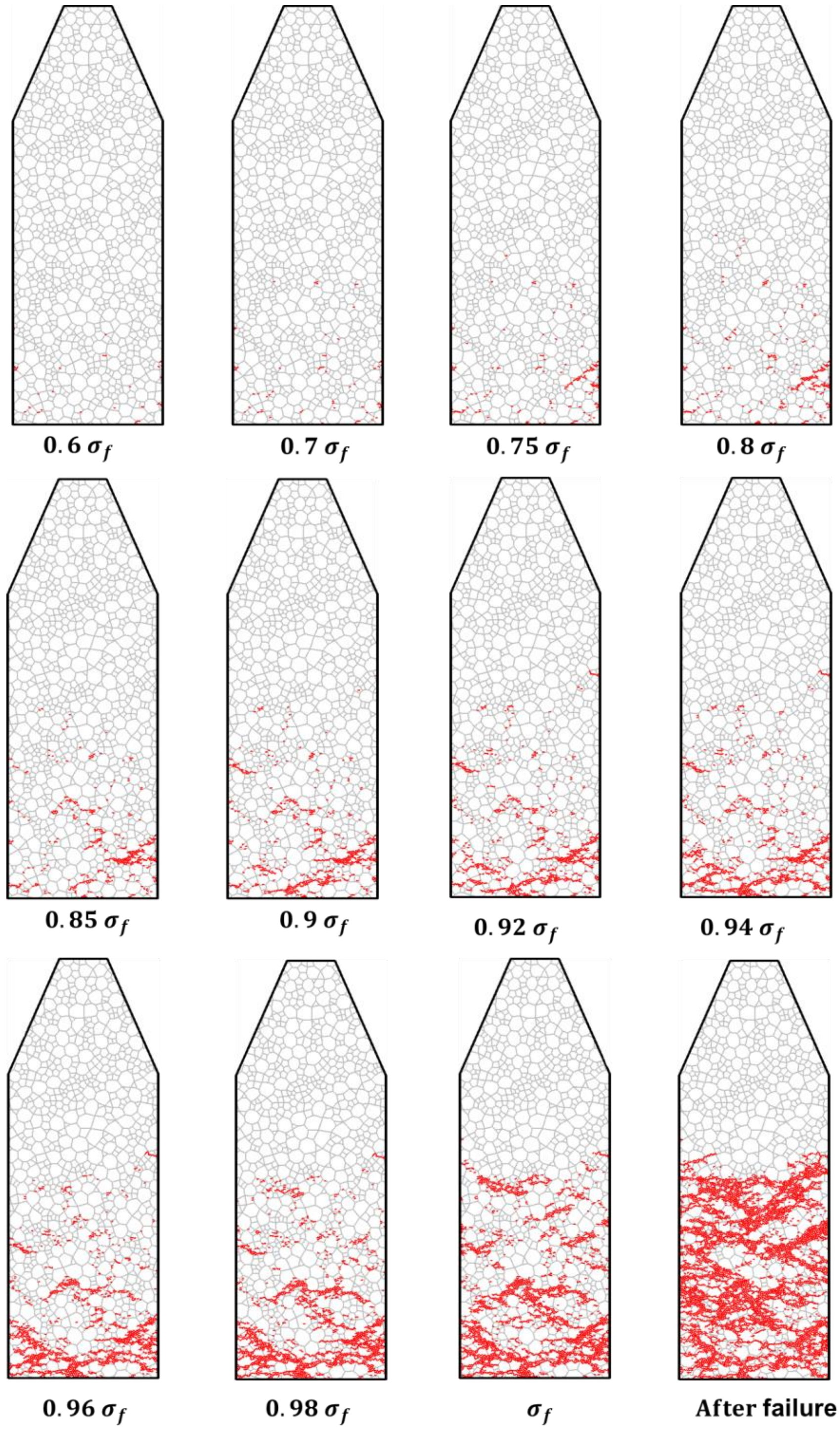

Figure S7. Results of numerical simulation (with particle flow model) for growth and propagation of microcracks in process of loading specimen to failure. $\boldsymbol{\sigma_f}$ represents the failure strength

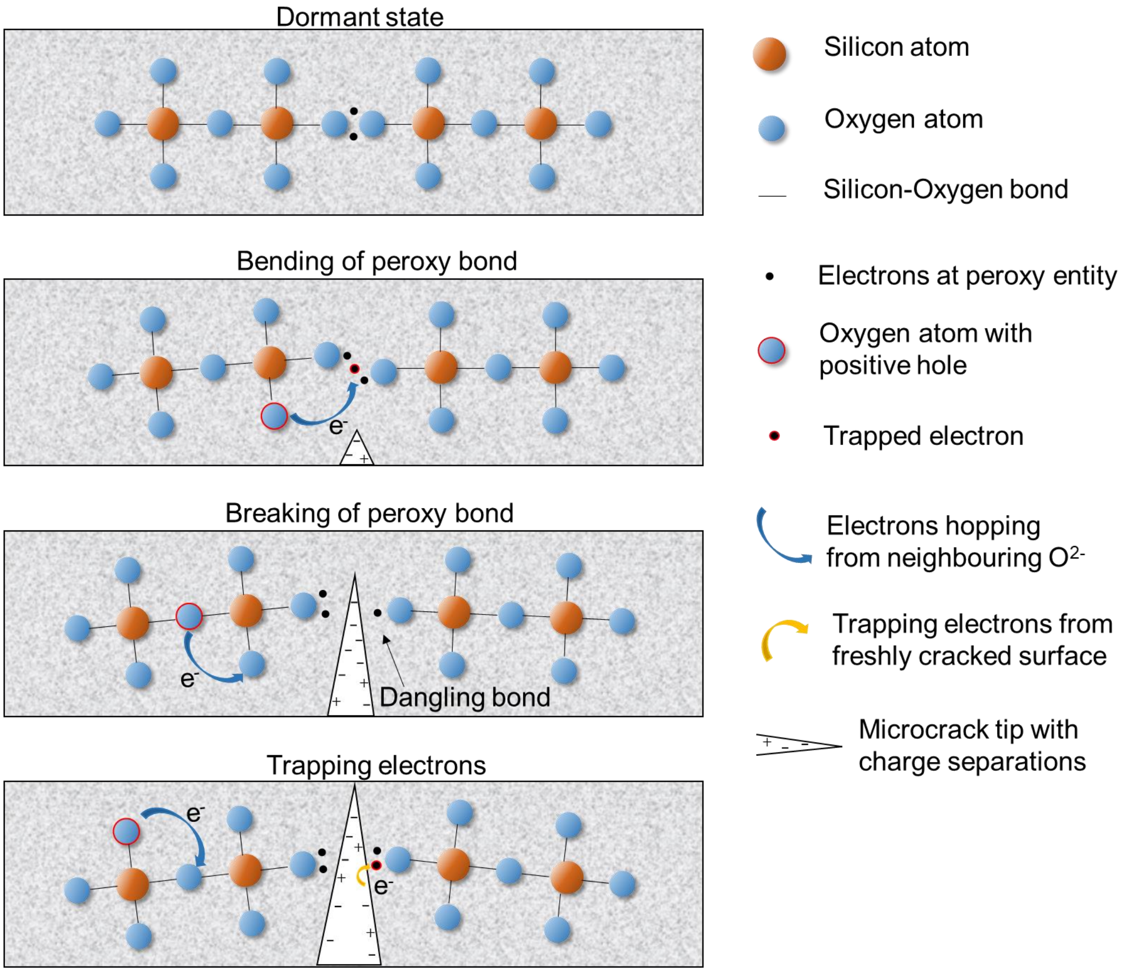

Figure S8. The schematic for illustrating the influences of growth of microcracks on the bending and breaking of proxy bond.

Specimen	σ_f (MPa)	*R*	ΔC_0 (nA)	ΔC_{1+}(nA)	$T_F - T_1$ (s)
S1	128.27	91.6%	+4.1	+114	0.48
S2	138.99	90.3%	+3	+53	0.78
S3	145.54	89.1%	+3	+96	0.89
S4	147.32	98.7%	+3.4	+115	1.11
S5	135.12	83.7%	+3.5	+199	0.64
S6	132.14	91.9%	+3.1	+682	0.61
S7	115.48	96.9%	+3.5	+203	0.95

R represents the strength ratio at which the PSRC of each specimen began to rise in a step-like way, ΔC_0 represents the increment amplitude of step-like rise in PSRC, ΔC_{1+} represents the increment amplitude of first positive fluctuations in PSRC prior to specimen failure, T_F represents the time of the specimen failure, T_1 represents the time of the first positive fluctuation in PSRC prior to specimen failure.

Table S1. The detected PSRC variations in experiments.

		Plagioclase	Hornblende	Pyroxene	Biotite
Physical properties					
Volume composite	V_{ratio}	60%	20%	10%	10%
Density	ρ (kg/m^3)	2620	3124	3260	3050
Modulus	E (GPa)	37.5	87	94.1	51
Poisson's ratio	μ	0.32	0.29	0.25	0.27
Sizes					
Minimum grain size	d_{min} (mm)	4.0	2.2	2.0	1.4
Maximum/Minimum	d_{max}/d_{min}	1.4	1.27	1.2	1.14

Table S2. Physical properties and size of particles for different mineral materials.

		Plagioclase	Hornblende	Pyroxene	Biotite
Balls					
Minimum radius	R_{min} (mm)	0.25			
Radius ratio	R_{max}/R_{min}	1.66			
Density	ρ (kg/m^3)	2620	3124	3260	3050
Young Modulus	E_{ball} (GPa)	33.5	68.0	78.0	56.0
Stiffness ratio	k_n/k_s	2.3	1.9	1.4	1.8
Friction coefficient	μ	0.5	0.5	0.5	0.5
Transgranular contacts					
Young Modulus	$E^{c}_{tra.}$ (GPa)	33.5	68.0	78.0	56.0
Stiffness ratio	$\bar{k}^{tra.}_{n}/\bar{k}^{tra.}_{s}$	2.3	1.9	1.4	1.8
Friction angle	$\varphi_{tra.}$ (degree)	10.0	15.0	15.0	10.0
Cohesion strength	$c_{tra.}$ (MPa)	100.0	80.0	110.0	50.0
Tension strength	$\sigma^{t}_{tra.}$ (MPa)	70.0	60.0	80.0	40.0
Intergranular contacts					
Linear Young Modulus	$E^{c}_{int.}$ (GPa)	20.0			
Linear stiffness ratio	$k^{int.}_{n}/k^{int.}_{s}$	2.9			
Parallel Young Modulus	$E^{pb}_{int.}$ (GPa)	20.0			
Parallel stiffness ratio	$\bar{k}^{int.}_{n}/\bar{k}^{int.}_{s}$	2.9			
Friction angle	$\varphi_{int.}$ (degree)	40.0			
Cohesion strength	$c_{tra.}$ (MPa)	35.0			
Tension strength	$\sigma^{int.}_{t}$ (MPa)	30.0			

Table S3. Calibrated parameters for different mineral materials in GB-DEM.

SI References

D. O. Potyondy. A grain-based model for rock: approaching the true microstructure. Proceedings of rock mechanics in the Nordic Countries, 9-12.